ACS OMEGA

http://pubs.acs.org/journal/acsodf

Article

Fe/Co-MOF Nanocatalysts: Greener Chemistry Approach for the Removal of Toxic Metals and Catalytic Applications

Fares T. Alshorifi,* Shady M. El Dafrawy, and Awad I. Ahmed

Cite This: *ACS Omega* 2022, 7, 23421−23444

Read Online

ACCESS | Metrics & More | Article Recommendations | Supporting Information

ABSTRACT: This study describes the preparation of new bimetallic (Fe/Co)−organic framework (Bi-MOF) nanocatalysts with different percentages of iron/cobalt for their use and reuse in adsorption, antibacterial, antioxidant, and catalytic applications following the principles of green chemistry. The prepared catalysts were characterized using several techniques, including X-ray powder diffraction, Fourier transform infrared spectroscopy, transmission electron microscopy, and scanning electron microscopy. These techniques proved the formation of MOFs, and the average crystallite sizes were 25.3−53.1, 27.6−67.2, 3.0−18.9, 3.0−12.9, and 3.0−23.6 nm for the Fe-MOF, Co-MOF, 10%Fe:90%Co-MOF, 50%Fe:50%Co-MOF, and 90%Fe:10%Co-MOF samples, respectively. The nanoscale (Fe/Co) Bi-MOF catalysts as efficient heterogeneous solid catalysts showed high catalytic activity with excellent yields and short reaction times in the catalytic reactions of quinoxaline and dibenzoxanthene compounds, in addition to their antioxidant and antibacterial activities. Furthermore, the nanoscale (Fe/Co) Bi-MOF catalysts efficiently removed toxic metal pollutants (Pb^{2+}, Hg^{2+}, Cd^{2+}, and Cu^{2+}) from aqueous solutions with high adsorption capacity.

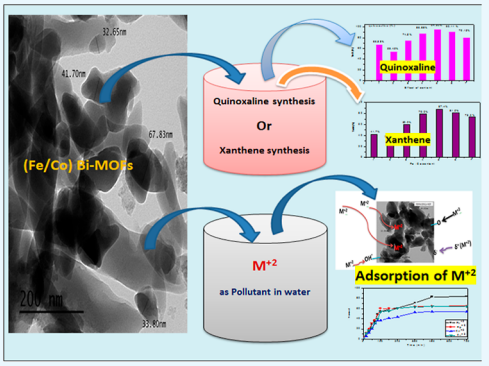

1. INTRODUCTION

Recently, the design, crystal engineering, and synthesis of metal−organic coordination frameworks have attracted great attention as promising functional materials. Metal−organic frameworks (MOFs) are a family of nonporous, crystalline solid-state materials with one-, two-, or three-dimensional structures.[1−3] MOFs are also known as coordination polymers,[4] and they are crystalline, microporous to mesoporous functional materials consisting of inorganic clusters interconnected by organic linkers.[5] Their inorganic components may be single or have more metal atoms coordinated by ligand atoms, and their organic components (ligand) are generally small organic molecules that can bind to metal ions or clusters via functional groups. Metal-linker clusters contain more than one metal atom or extended arrays of metal atoms linked by single ligand atoms.[6,7]

Because of their unique characteristics (e.g., high specific surface area, high porosity, controllable pore size, low density, and great functionality), intriguing architectures, and intricate entangled motifs, MOFs have a wide range of applications in gas storage, gas separation, heterogeneous catalysis, microelectronics, nonlinear optics, sensing, drug delivery, membranes, and pollutant adsorption.[8−14] MOFs have many advantages over the more widely known zeolites.[15] Compared with traditional porous materials, MOFs have high specific surface areas, reaching about 10,000 m^2/g.[13] Although MOFs are relatively new, their basic structures, known as the secondary building unit,[16] very closely resemble those of metal complexes as organic linkers can donate multiple lone pairs of electrons to metal cations, whereas metal cations are made up of vacant orbital shells that can accept these lone pairs of electrons to form MOFs.[17]

A general strategy for the utilization of heterometallic−organic frameworks, especially bimetallic−organic frameworks (Bi-MOFs), is the use of two or more different metals.[18,19] On the subject of the catalytic activities of coordination polymers (MOFs), the types and properties of incorporated metal ions are important.[20−23] In principle, the active sites of MOF catalysts can be the metals at the nodes of a framework (metal centers with unsaturated coordination environments).[23,24] In MOF compounds, the metal ions and organic linker (ligand) play important roles in catalytic reaction mechanisms. The inorganic metal moieties are Lewis acids; that is, they can act as electron pair acceptors, especially when uncoordinated metal sites are generated because of the removal of coordinated solvent molecules that remain after the preparation of MOFs.[10,25]

The synthesis of multi-MOFs as nanomolds for hosting functional inorganic nanoparticles and their wide application have attracted attention in the last few years.[19,22,26] In this

Received: March 23, 2022
Accepted: June 14, 2022
Published: June 27, 2022

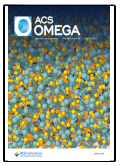

regard, heavy metals are of great concern because of the continuous industrial development. However, the intensive spread and accumulation of contaminants in water are considered serious environmental problems affecting human, animal, and plant life when released into the environment.[27−30] For instance, lead, mercury, copper, and cadmium ions are considered the worst heavy metals for humans and animals.[31−33]

Quinoxaline and its derivatives are fragments of several biologically active and pharmacologically important compounds.[34] It exhibits a broad spectrum of biological activities (e.g., antibacterial, antiviral, anticancer, antifungal, antitubercular, and anti-inflammatory).[35−38] In recent years, the use of recoverable and reusable catalysts has attracted special attention because of their nontoxicity and economic, environmental, and industrial advantages.[39] For instance, xanthene and its derivatives are important because of their wide range of biological and pharmaceutical characterizations and have agricultural bactericidal, antiviral, anti-inflammatory, and antiviral activities.[40−44] They have been widely used in dyes, fluorescent materials for the visualization of biomolecules, and laser technologies. However, many of the synthesis methods of these catalysts suffer from one or more disadvantages, such as long reaction times (from 16 h to 5 days), harsh conditions, expensive reagents, use of toxic organic solvents, low product yields, and the need for excess reagents and catalysts.

This work aims to further understand new (Fe/Co) Bi-MOF nanocatalysts to determine their potential use in adsorption, antibacterial, antioxidant, and catalytic applications. Particular focus was devoted to the synthesis, structural characterization, and different applications of new inorganic−organic frameworks consisting of two different metals to investigate their diversity and potential as functional materials. We used the prepared nanocatalysts for the adsorption removal of four different heavy metals, catalytic activity of quinoxaline and dibenzoxanthene compounds, and antibacterial and antioxidant activities. Following the principles of green chemistry, the design of easily separable, reusable, nontoxic, low-cost, and insoluble acidic (Fe/Co) Bi-MOF nanocatalysts is the most important aim of this work.

2. EXPERIMENTAL SECTION

2.1. Preparation of the Catalyst Samples. *2.1.1. Preparation of Fe-MOF Nanoparticles.* The Fe-MOF was synthesized using the solvothermal method by mixing $Fe(NO_3)_3{\cdot}9H_2O$ and terephthalic acid (1:1 M ratio M/L) in 40 mL of dimethylformamide (DMF) under vigorous stirring, followed by the addition of 2.2 mL of triethylamine dropwise. The mixture was stirred for 2 h and then transferred into a Teflon-lined autoclave, which was sealed and maintained at 120 °C for 4 h. A brownish precipitate was formed and then filtered by centrifugation, washed, added to chloroform, and left overnight. Thereafter, the precipitate was filtered and dried at 60 °C in a vacuum oven for 6 h.[1,12,45]

2.1.2. Preparation of Co-MOF Nanoparticles. The Co-MOF was synthesized using the solvothermal method by mixing $Co(NO_3)_2{\cdot}6H_2O$ and terephthalic acid (1:1 M ratio M/L) in 40 mL of DMF under vigorous stirring, followed by the addition of 2.2 mL of triethylamine dropwise. The mixture was stirred for 2 h and then transferred into a Teflon-lined autoclave, which was sealed and maintained at 120 °C for 4 h. A purple precipitate was formed and then filtered by centrifugation, washed, added to chloroform, and left overnight. Thereafter, the precipitate was filtered and dried at 60 °C in a vacuum oven for 6 h.[45−48]

2.1.3. Preparation of (Fe/Co) Bi-MOF Nanoparticles. Bi-MOFs (10%Fe:90%Co, 30%Fe:70%Co, 50%Fe:50%Co, 70% Fe:30%Co, and 90%Fe:10%Co) were synthesized using the solvothermal method by mixing $Co(NO_3)_2{\cdot}6H_2O$ and $Fe(NO_3)_3{\cdot}9H_2O$ with terephthalic acid (1:1 M ratio M/L) in 40 mL of DMF under vigorous stirring, followed by the addition of 2.2 mL of triethylamine dropwise. The mixture was stirred for 2 h and then transferred into a Teflon-lined autoclave, which was sealed and maintained at 120 °C for 4 h. A precipitate was formed and then filtered by centrifugation, washed, added to chloroform, and left overnight. Thereafter, the precipitate was filtered and dried at 60 °C in a vacuum oven for 6 h.[8,11,12,22,45−53]

2.2. (Fe/Co) Bi-MOF Nanocatalyst Applications. *2.2.1. Adsorption Activity.* Adsorption studies were performed using 0.03 g of activated Fe-MOF, Co-MOF, and (Fe/Co) Bi-MOF nanocatalysts and 100 ppm/100 mL of heavy metal solutions (lead, copper, mercury, and cadmium) for 120 min. The pH values of the pollutant solutions were adjusted to 2−7 or 8 for heavy metals using 0.1 M HCl and 0.1 M NaOH solutions. The heavy metal equilibrium concentrations were determined using the spectrophotometric method at a certain wavelength for each pollutant. The adsorbed amount of heavy metals at equilibrium (q_e in mg/g) was calculated using the following equation

$$q_e = \frac{[(C_0 - C_e)V]}{W_t} \quad (1)$$

and

$$\%\text{removal} = \frac{[C_0 - C_t]}{C_0} \times 100 \quad (2)$$

2.2.2. Catalytic Activity. Quinoxaline was synthesized using a mixture of 0.1 mol *o*-phenylenediamine and 0.1 mol diethyl oxalate in a round flask. Then, the flask was placed in an oil bath and refluxed for 2 h at 80 °C in the presence of 0.03 g of activated (Fe/Co) Bi-MOF nanocatalysts.[37,39,54] Dibenzoxanthene was synthesized using a mixture of 2 mmol β-naphthol with 1 mmol benzaldehyde in a round flask. The flask was then placed in an oil bath and refluxed for 30 min at 70 °C in the presence of 0.03 g of activated (Fe/Co) Bi-MOF nanocatalysts.[41,44,55,56] The formed solid was filtered, washed with water, and dried to give a pure compound. It could be also purified by crystallization from ethanol. The product was characterized by thin-layer chromatography (TLC) and Fourier transform infrared (FTIR) spectroscopy.

2.2.3. Antibacterial and Antioxidant Activities. We studied the antibacterial and antioxidant activities of all the nanocatalyst samples, where the antibacterial activities of the prepared nanocatalysts were individually tested against a panel of Gram-positive *Bacillus subtilis*, Gram-negative *Escherichia coli*, and *Candida barbicans*.

3. RESULTS AND DISCUSSION

3.1. X-ray Diffraction Analysis. Figure 1 shows the X-ray diffraction (XRD) patterns of the different percentages of (Fe/Co) Bi-MOF catalysts. The peaks of the Fe-MOF catalysts appeared at 5.34, 6.73, 9.63, 11.60, 12.88, 13.67, 14.80, 20.30, 23.34, 24.23, 25.25, 29.07, 34.68, 35.92, 37.49, 44.12, and 46.25°, indicating that the Fe-MOF catalysts were crystal-

https://doi.org/10.1021/acsomega.2c01770
ACS Omega 2022, 7, 23421−23444

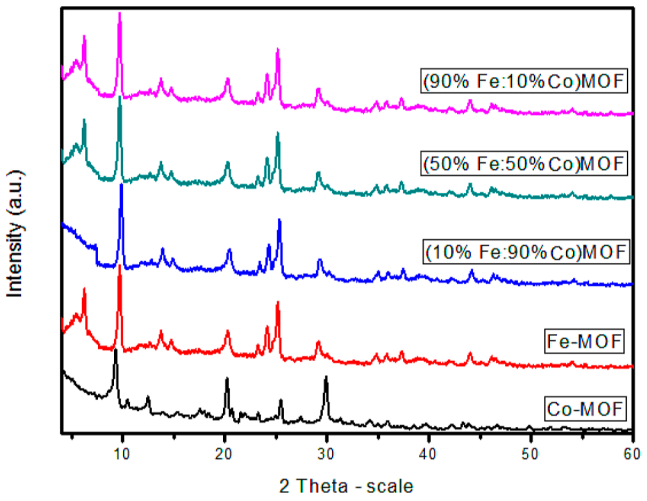

Figure 1. XRD pattern of Fe-MOF, Co-MOF, 10%Fe:90% Co-MOF, 50% Fe:50%Co-MOF, and 90% Fe:10%Co-MOF samples.

lized.[51,52] The peaks of the Co-MOF catalysts appeared at 9.29, 10.56, 12.56, 15.35, 17.60, 20.19, 21.76, 23.34, 25.45, 27.94, 29.85, 34.35, 36.03, and 33.67°, indicating that the Co-MOF catalysts were crystallized.[47,49] The XRD patterns of Co-MOF showed two main peaks at 9.29 and 20.19°, which corresponds to a standard pattern.[49] The main peaks of the 10%Fe:90%Co-MOF, 50%Fe:50%Co-MOF, and 90%Fe:10% Co-MOFs appeared at 5.35, 6.23, 9.74, 13.74, 14.79, 20.10, 24.30, 23.23°, 24.23, 25.35, 29.28, 34.90, 35.92, 37.37, 43.90, and 46.25°,[22,50−53,57] indicating that all (Fe/Co) Bi-MOF samples were crystallized. We observed that the peak at 9.63° of the Fe-MOF catalyst was stronger than that of the Co-MOF catalyst. The XRD patterns show that the peak at 9.29° increased with the increase in the iron percentage from 10 to 90% in the (Fe/Co) Bi-MOFs. The peak at 29.00° was clearer in the Co-MOF catalyst, which slightly decreased with the increased percentage of iron in the (Fe/Co) Bi-MOF catalysts. Generally, the peaks of the Fe-MOF increased with the increasing percentages of iron in the (Fe/Co) Bi-MOF catalysts, whereas the peak of the Co-MOF decreased with the decreasing percentages of cobalt in the (Fe/Co) Bi-MOF catalysts (i.e., the peaks of the Co-MOF catalysts decreased with the increasing percentages of iron). A sharp peak below 10° indicated that the MOF materials are crystalline. These results confirm the formation of (Fe/Co) Bi-MOFs and are in good agreement with the results of Wang et al.[50] The crystallite sizes were 25.3−53.1, 27.6−67.2, 3.0−18.9, 3.0−12.9, and 3.0−23.6 nm for Fe-MOF, Co-MOF, 10%Fe:90%Co-MOF, 50%Fe:50%Co-MOF, and 90%Fe:10%Co-MOF, respectively.

3.2. FTIR Spectroscopy. The prepared catalysts were characterized using their FTIR spectra. Fe-MOF, Co-MOF, 10%Fe:90%Co-MOF, 30%Fe:70%Co-MOF, 50%Fe:50%Co-MOF, 70%Fe:30%Co-MOF, and 90%Fe:10%Co-MOF samples were observed at room temperature to confirm the presence of BTC (to confirm the formation of MOFs), as shown in Figure 2. The peaks at 1663 and 1579 and 1478 and 1384 cm^{-1} indicate asymmetric and symmetric carboxylate groups, respectively.[2,48,58] Additionally, the absence of a strong absorption band near 1710 or 1714 cm^{-1} indicates that all carboxyl groups of the terephthalic ligand are deprotonated.[11,48,59] The broad and medium-intensity peak at 3420−3432 cm^{-1} was produced by the (OH) stretching vibrations of coordinated water molecules.[59,60] The $\Delta\nu$ [ν_{as}(COO) − ν_{s}(COO)] values were 185 and 195 cm^{-1}, which are characteristic of the bridge coordination mode.[50,60] The relatively weak absorption band located at 3063 cm^{-1} was due to the stretching vibrations of the aromatic ring $-(CH)_{ar}$, which confirms the presence of ligand molecules in the MOFs.[53,61] Additionally, the peak at 1105−1111 cm^{-1} was related to the C−O stretching vibration.[50,61] Generally, most of the bands in the region from about 1600−1605 to 700−800 cm^{-1} were due to aromatic ring stretching. The weak and

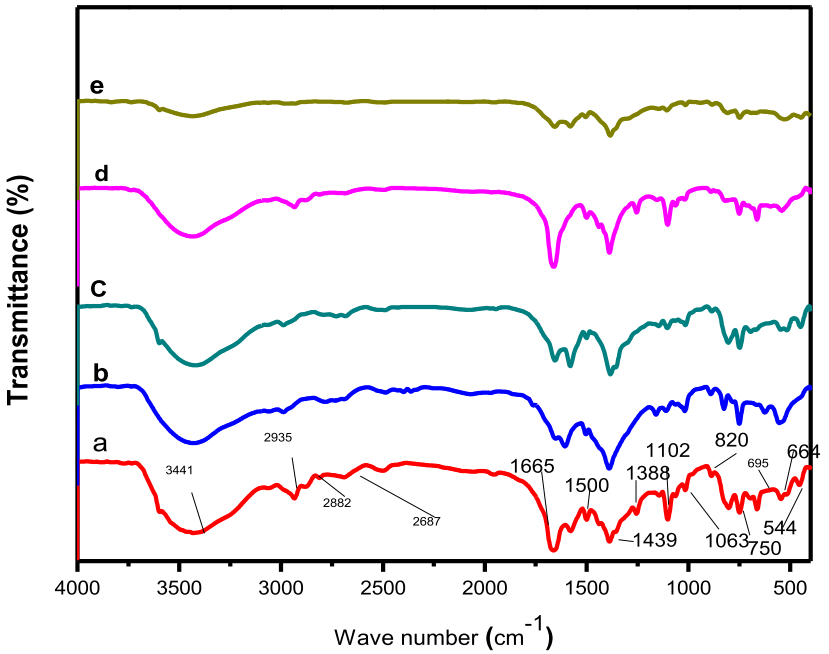

Figure 2. FTIR spectra of (a) Co-MOF, (b) Fe-MOF, (c) (10%Fe:90%Co)-MOF, (d) (50% Fe:50%Co)-MOF, and (e) (90% Fe:10%Co)-MOF samples.

https://doi.org/10.1021/acsomega.2c01770
ACS Omega 2022, 7, 23421−23444

narrow bands at 1065−1083 and 750−782 cm^{-1} could be attributed to the γ(C−H) and δ(C−H) vibration of aromatic rings, respectively.[62] The band with medium strength at 538−557 cm^{-1} was due to M−O vibrations, which proved that MOFs were indeed formed.[61]

3.3. Transmission Electron Microscopy. Figure 3 shows the transmission electron microscopy (TEM) images of the

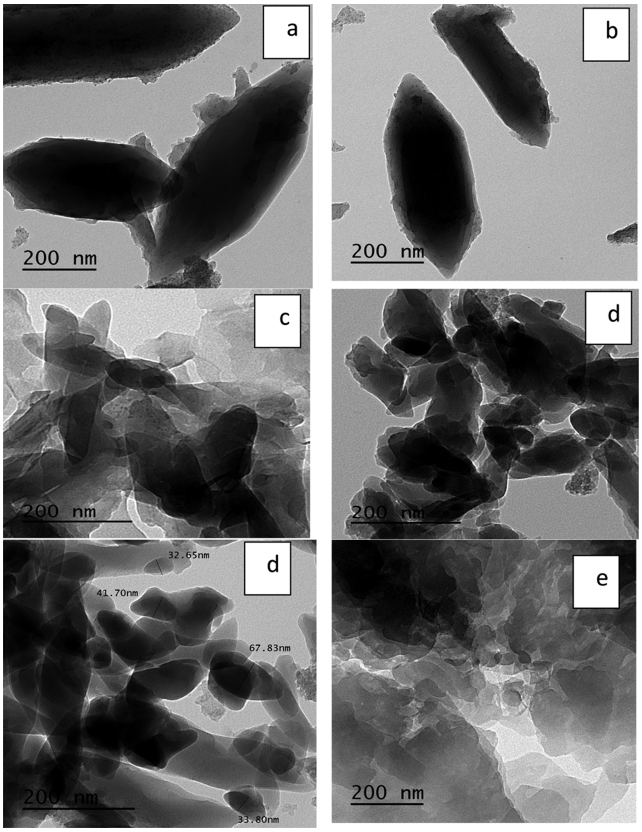

Figure 3. TEM images of (a) Fe-MOF, (b) Co-MOF, (c) 10% Fe:90% Co-MOF, (d) 50% Fe:50%Co-MOF, and (e) 90% Fe:10% Co-MOF samples.

morphology and microstructure of Fe-MOF, Co-MOF, and (Fe/Co)-MOF catalysts. The results showed irregular and similar hexagonal particles with nanosizes reaching nearly 28.8 and 27.6 nm for the Fe-MOF and Co-MOF, respectively. The TEM images of the 10%Fe:90%Co-MOF, 50%Fe:50%Co-MOF, and 90%Fe:10%Co-MOF catalysts showed the presence of two different shapes with defects in the (Fe/Co)-MOF samples, with nanosizes reaching nearly 23.0, 22.9, and 23.6 nm for 10%Fe:90%Co-MOFs, 50%Fe:50%Co-MOFs, and 90% %Fe:10%Co-MOFs, respectively. These results are in accordance with the XRD results. The 50%Fe:50%Co-MOFs showed an enhanced crystallinity with a crystallite size of 22.9 nm, making it the best nanosize sample with high catalytic and adsorption activities.

3.4. Scanning Electron Microscopy. Figure 4 shows the scanning electron microscopy (SEM) images of the MOF samples, which show irregular and similar hexagonal particles with smooth and large surface areas and nanosizes reaching nearly 28.8 and 27.6 nm for the Fe-MOF and Co-MOF, respectively. They also show large surface areas and the presence of two different shapes for the (Fe/Co) Bi-MOF samples with defects for 10%Fe:90%Co-MOF, 50%Fe:50%Co-

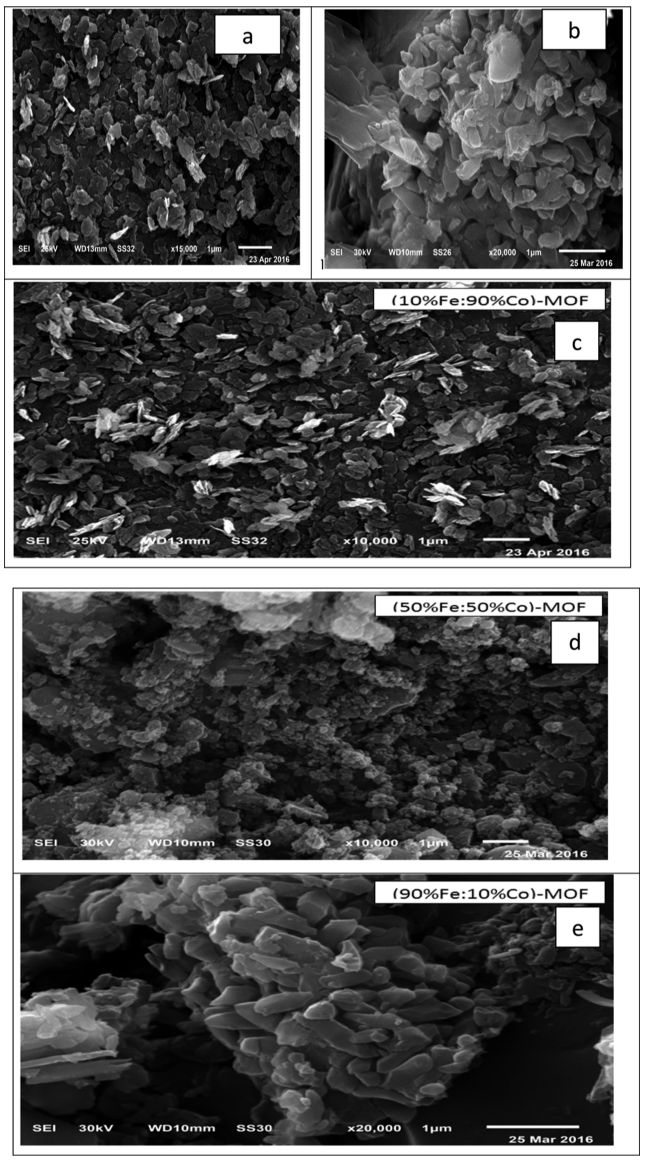

Figure 4. SEM images of (a) Fe-MOF, (b) Co-MOF, (c) 10%Fe:90% Co-MOF, (d) 50%Fe:50%Co-MOF, and (e) 90% Fe:10%Co-MOF samples.

MOF, and 90%%Fe:10%Co-MOF with nanosizes reaching nearly 23.0, 22.9, and 23.6 nm, respectively, which are in accordance with the XRD and TEM results.

3.5. Adsorption Activity. This section reports the adsorption of heavy metals (Pb^{2+}, Hg^{2+}, Cd^{2+}, and Cu^{2+}) as environmental pollutants from aqueous solutions.

3.5.1. Effect of pH on Adsorption. The pH of pollutant solutions is one of the major factors that influence the adsorption of heavy metals.[63] We studied the influence of pH on the removal of Pb(II), Hg(II), Cd(II), and Cu(II) using (Fe/Co) Bi-MOFs, presented in Figure 5. Generally, the uptake of Pb(II), Hg(II), Cu(II), and Cd(II) ions on absorbents by 0.03 g of Bi-MOF catalysts placed in bottles containing 100 mL of aqueous solutions of heavy metals as inorganic pollutants was significantly high in basic solutions compared with that in acidic solutions at an initial concentration (100 mg/L). The pH values selected in the experiments were prior to the precipitation limit of metals: pH = 5 for Pb^{2+}, pH = 7 for Cd^{2+}, and pH = 6 for Cu^{2+} and Hg^{2+}.

https://doi.org/10.1021/acsomega.2c01770
ACS Omega 2022, 7, 23421−23444

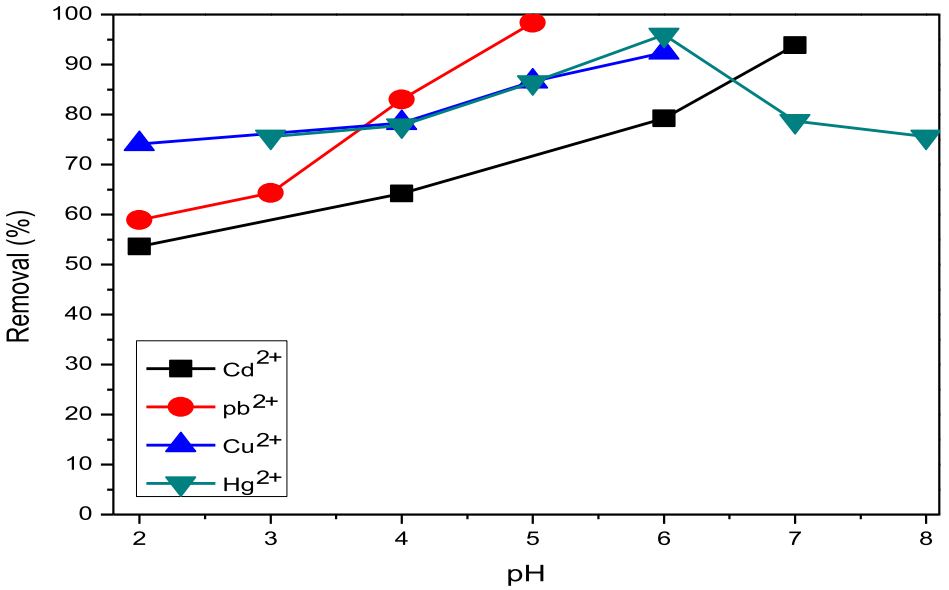

Figure 5. Effect of pH on the adsorption of Cd^{2+}, Pb^{2+}, Cu^{2+}, and Hg^{2+} after 120 min using 0.03 g of the 50%Fe:50%Co-MOF nanocatalyst.

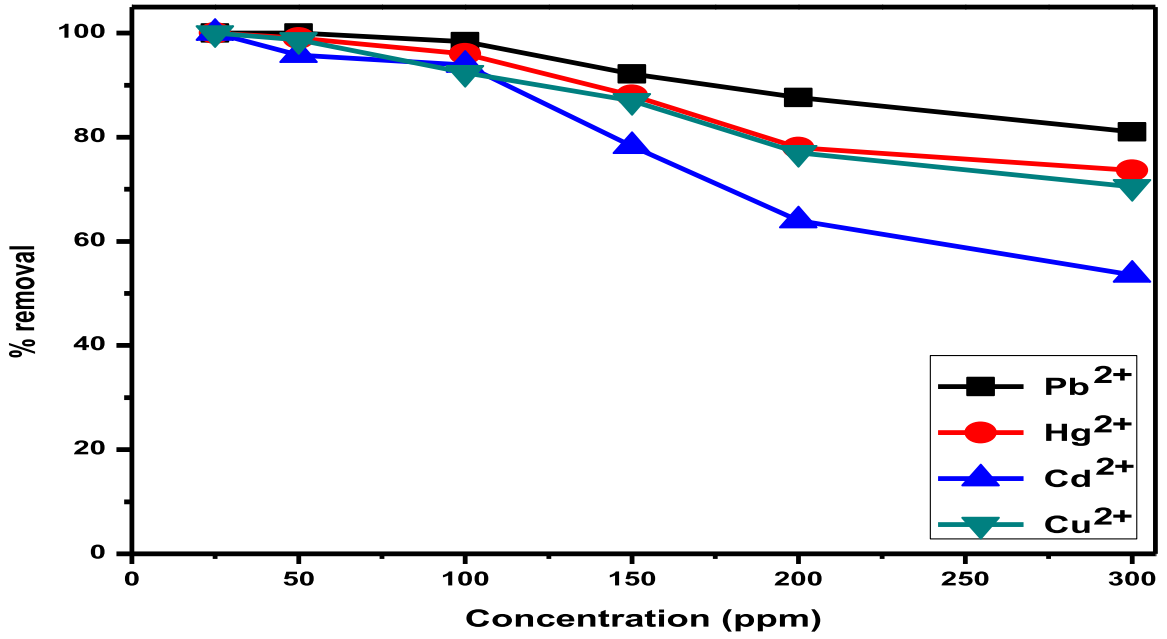

Figure 6. Effect of initial metal concentrations on the adsorption of Cd^{2+}, Pb^{2+}, Cu^{2+}, and Hg^{2+} after 120 min using 0.03 g of the 50%Fe:50%Co-MOF nanocatalyst.

In Figure 5, the maximum adsorption capacities were 98.89, 95.98, 93.89, and 92.6% for lead, mercury, cadmium, and copper ions, respectively, on the Bi-MOF samples after 120 min. At low pH values, low removal efficiencies were observed because of hydrogen ions competing with metal ions on active sites (at ion-exchangeable sites).[64,65] The protonation of the surface of the catalysts at a lower pH led to the extensive repulsion of metal ions, which may be another reason for the decrease in the adsorption of metals at lower pH ranges.

3.5.2. Effect of Initial Metal Concentrations on Adsorption. We studied the effects of the initial concentrations of lead, mercury, cadmium, and copper ions on the removal rate at initial concentrations of 25, 50, 100, 150, 200, and 300 mg/L after 120 min using 0.03 g of the 50%Fe:50%Co-MOF nanocatalyst. Figure 6 shows the adsorption capacities of heavy metals. The removal percentage decreased with the increase in initial concentrations of heavy metals from 25 to 300 mg/L. Evidently, at C_o = 25, 50, 100, 150, 200, and 300 mg/L, the maximum adsorption capacities on the 50%Fe:50%Co-MOF nanocatalyst after 120 min were 100, 100, 98.37, 92.16, 87.65, and 81.01% for lead ions; 100, 99.045, 95.98, 88.01, 78.00, and 73.63% for mercury ions; 100, 95.75, 93.89, 78.3, 64.02, and 53.55% for cadmium ions; and 100, 98.70, 92.40, 87.00, 76.99, and 70.50% for copper ions, respectively. At lower solution concentrations, the removal percentage was about 100% (i.e., approaching complete removal of heavy metals), which is highly appreciated in some cases such as the treatment of metal pollutants from wastewater. The decrease in the removal percentage of heavy metals at C_0 = 300 mg/L may be attributed to the saturation of available active sites on the

https://doi.org/10.1021/acsomega.2c01770
ACS Omega 2022, 7, 23421−23444

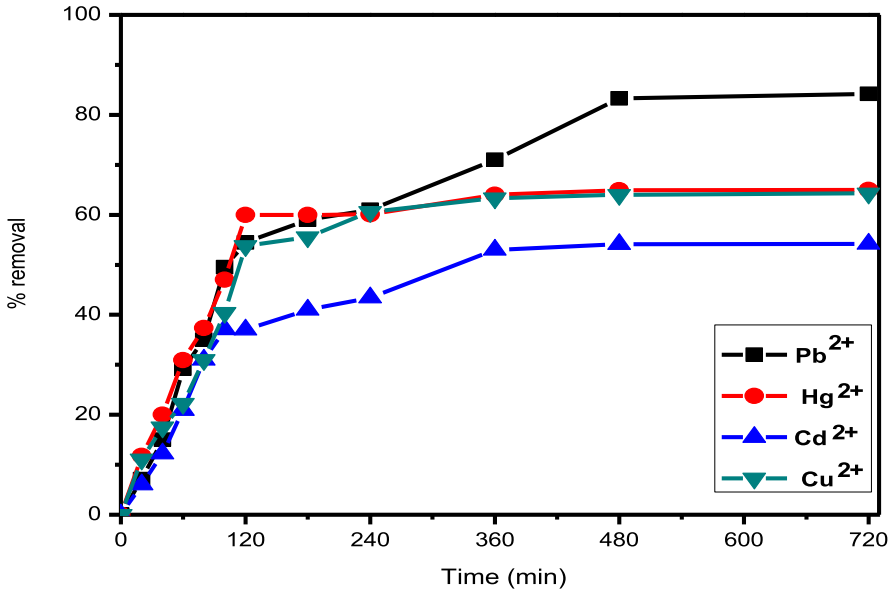

Figure 7. Effect of contact time on the adsorption of Cd^{2+}, Pb^{2+}, Cu^{2+}, and Hg^{2+} after 12 h by the Fe-MOF sample.

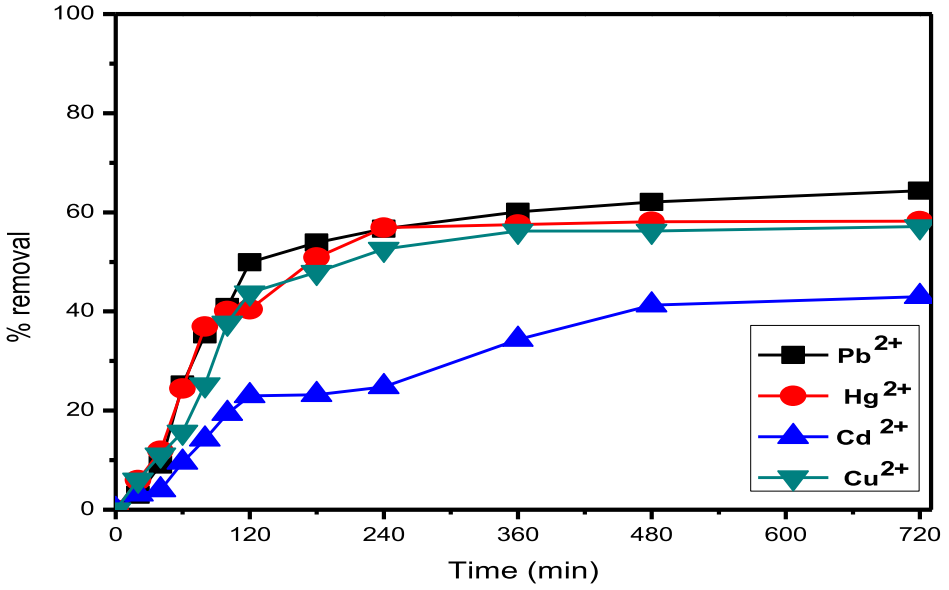

Figure 8. Effect of contact time on the adsorption of Cd^{2+}, Pb^{2+}, Cu^{2+}, and Hg^{2+} after 12 h by the Co-MOF sample.

surface of the catalysts with the increase in the initial concentrations of heavy metals.[30,31,66,67] Additionally, the metal salt solutions contained nitrate or chloride anions, which increased in the metal solutions with increasing metal concentrations. In other words, the increase in the nitrate or chloride ions may block the active sites of the catalyst surfaces.

3.5.3. Effect of Adsorption Kinetics on the Adsorption of Heavy Metals. The adsorption efficiency as a function of contact time was monitored by varying the equilibrium time between the adsorbate (heavy metals) and the adsorbent (the prepared catalysts) in the range of 0−120 min for Fe-MOF, Co-MOF, 10%Fe:90%Co-MOF, 30%Fe:70%Co-MOF, 50% Fe:50%Co-MOF, 70%Fe:30%Co-MOF, and 90%Fe:10%Co-MOF samples. The effect of the content time on the adsorption of lead, mercury, cadmium, and copper ions onto the prepared catalysts was determined at an initial concentration of 100 mg/L at 25 °C using 0.03 g of the nanocatalysts. The time required to reach equilibrium is 6 h for the Fe-MOF and Co-MOF nanocatalysts and 120 min for the Bi-MOF nanocatalysts. Figures 7−12 show the effect of contact time on the adsorption of heavy metals. The removal of metal ions on the Fe-MOF and Co-MOF nanocatalysts observed a quick increase during the first 4 h and then a gradual increase within 6 h. Thereafter, no or a slight increase in metal adsorption was observed. For the removal of metal ions on the Bi-MOF nanocatalysts, a quick increase within the first 60 min, then a gradual increase within 120 min, and no able increase in the adsorption of heavy metals thereafter were observed. The experimental data confirmed that the 50%Fe:50%Co-MOF was the best sample for the adsorption of heavy metals. The uptake expressed in terms of the amount of the metal removed from the pollutant solutions was as follows: Pb (II) > Hg(II) > Cd(II) > Cu(II).

3.5.4. Effect of Catalyst Dosage. The adsorption of lead, mercury, cadmium, and copper cations by the (Fe/Co) Bi-MOF nanocatalysts was studied by changing the amount of the

https://doi.org/10.1021/acsomega.2c01770
ACS Omega 2022, 7, 23421−23444

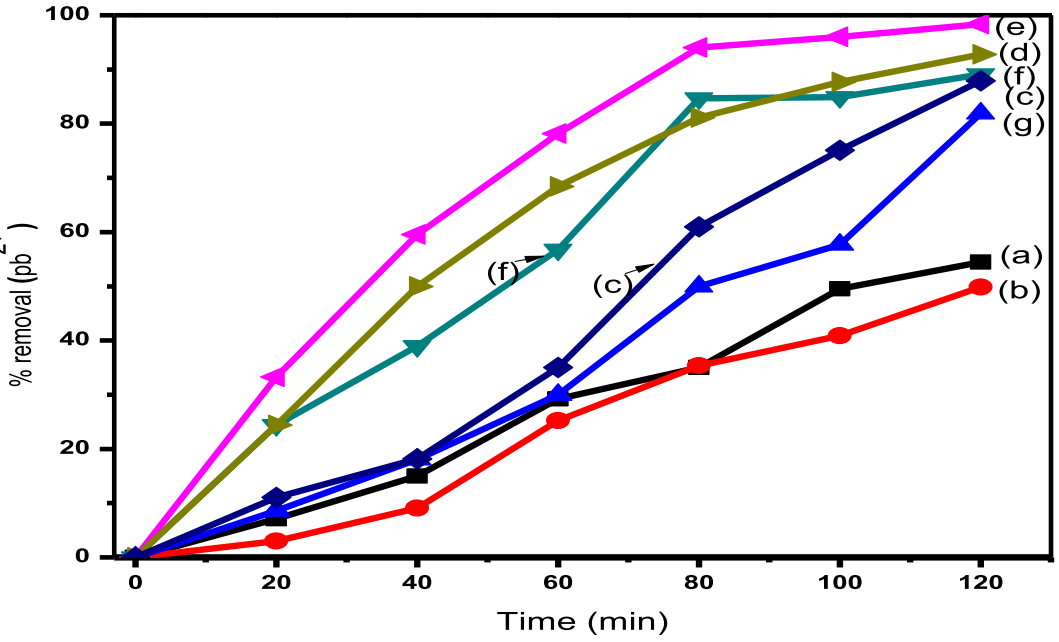

Figure 9. Effect of contact time on the adsorption of Pb^{2+} by (a) Fe-MOF, (b) Co-MOF, (c) 10%Fe:90%Co-MOF, (d) 30%Fe:70%Co-MOF, (e) 50%Fe:50%Co-MOF, (f) 70%Fe:30%Co-MOF, and (g) 90%Fe:10%Co-MOF samples.

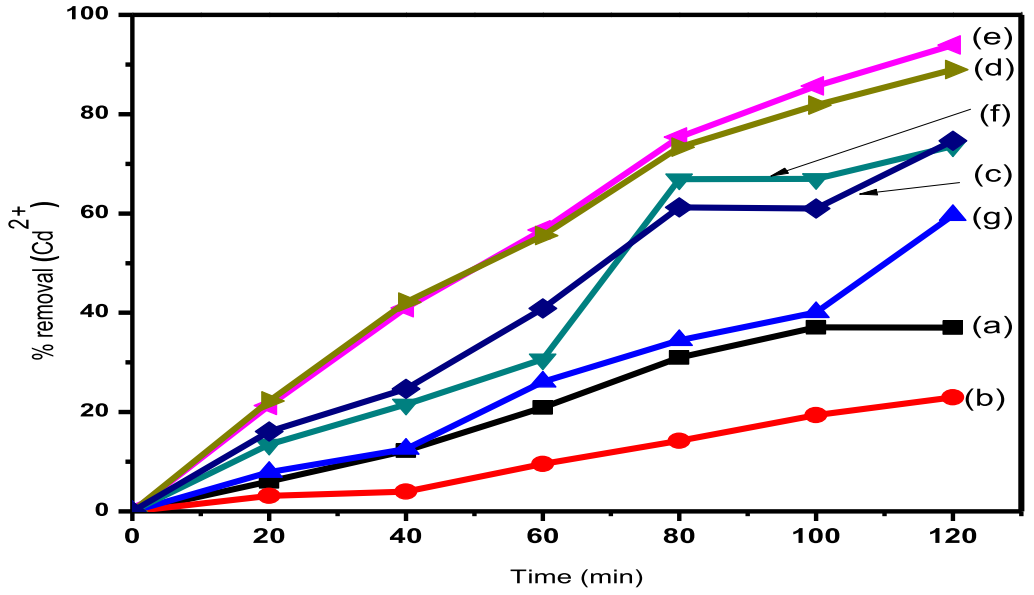

Figure 10. Effect of contact time on the adsorption of Cd^{2+} by (a) Fe-MOF, (b) Co-MOF, (c) 10%Fe:90%Co-MOF, (d) 30%Fe:70%Co-MOF, (e) 50%Fe:50%Co-MOF, (f) 70%Fe:30%Co-MOF, and (g) 90%Fe:10%Co-MOF samples.

catalyst (0.01, 0.03, 0.05, and 0.07 g) but keeping the initial metal concentration at 100 mg/L for 120 min on the 50% Fe:50%Co-MOF sample. The effect of the catalyst weight on the removal of Pb^{2+}, Hg^{2+}, Cd^{2+}, and Cu^{2+} ions is presented in Figure 13. The results reveal that the removal percentage of the toxic heavy metals from aqueous solutions increased with the increase in the catalyst weight from 0.01 to 0.07 g. The maximum adsorption efficiencies for 0.07 g of the 50%Fe:50% Co-MOF nanocatalyst after 120 min were 100, 99.37, 98.45, and 98.11% for lead, mercury, cadmium, and copper ions, respectively. This indicates that as the amount of the (Fe/Co) Bi-MOF nanocatalysts is increased, their ability to adsorb metals increases. This is because surfaces are finite at low catalyst weights, whereas they are infinite at high weights.[68]

3.5.5. Effect of the Repeated Use of Catalysts. Figure 14 shows the effect of reusing catalysts on heavy metal adsorption using 0.03 g of the 50%Fe:50%Co Bi-MOF. The adsorption activity slightly decreased with catalyst reuse from 98.37, 95.98, 93.89, and 92.60% at the first use to about 60.11, 52.09, 46.89, and 50.31% at the fourth use for lead, mercury, cadmium, and copper ions, respectively. This clearly indicates the slight deactivation of the catalysts possibly because of the presence of nitrates or chlorides originating from the solutions of the metal salts or the gradual loss of weight of the catalysts during filtration and washing.[68] Our recyclability studies suggest that the prepared catalysts can be repeatedly used as efficient adsorbents in water treatment.

https://doi.org/10.1021/acsomega.2c01770
ACS Omega 2022, 7, 23421−23444

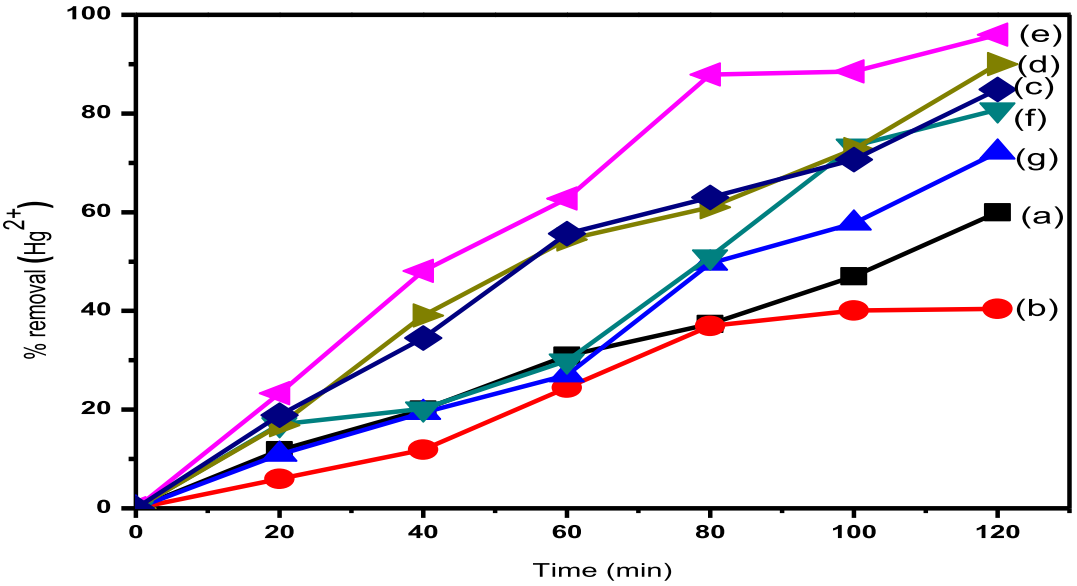

Figure 11. Effect of contact time on the adsorption of Hg^{2+} by (a) Fe-MOF, (b) Co-MOF, (c) 10%Fe:90%Co-MOF, (d) 30%Fe:70%Co-MOF, (e) 50%Fe:50%Co-MOF, (f) 70%Fe:30%Co-MOF, and (g) 90%Fe:10%Co-MOF samples.

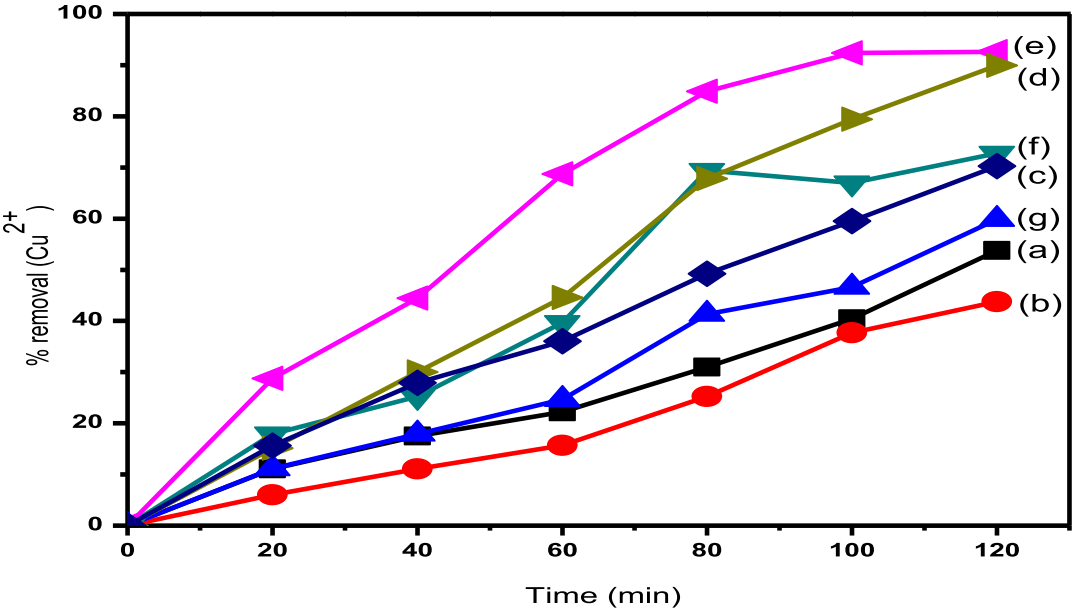

Figure 12. Effect of contact time on the adsorption of Cu^{2+} by (a) Fe-MOF, (b) Co-MOF, (c) 10%Fe:90%Co-MOF, (d) 30%Fe:70%Co-MOF, (e) 50%Fe:50%Co-MOF, (f) 70%Fe:30%Co-MOF, and (g) 90%Fe:10%Co-MOF samples.

3.5.6. Adsorption Isotherms. The study of adsorption isotherms is very important in determining the correlations between adsorbates and adsorbents at equilibrium conditions. Thus, we used several adsorption isotherm models with distinguished parameters to understand the adsorption mechanism behavior of the adsorbent surface during adsorption and its adsorption capacity to adsorb adsorbates (pollutants).[66] We used in this study two widely used adsorption isotherm models: the Langmuir[69] and Freundlich[70] models.

The Langmuir and Freundlich isotherms equations can be written as follows

Langmuir equations

$$\frac{C_e}{q_e} = \frac{1}{K_L q_m} + \frac{C_e}{q_m} \quad (3)$$

$$\log q_e = \frac{1}{n}\log C_e + \log K_F \quad (4)$$

where q_m (mg/g) is the maximum amount of pollutants (heavy metals) that can be adsorbed, K_L is the Langmuir constant related to adsorption rates, K_F is the Freundlich constant, and n indicates the favorability of the adsorption process. For the Langmuir isotherm, a straight line with slope = $\frac{1}{q_m}$ and intercept = $\frac{1}{Kq_m}$ is obtained by plotting C_e/q_e against C_e. One of the essential characteristics of the Langmuir isotherm model

https://doi.org/10.1021/acsomega.2c01770
ACS Omega 2022, 7, 23421−23444

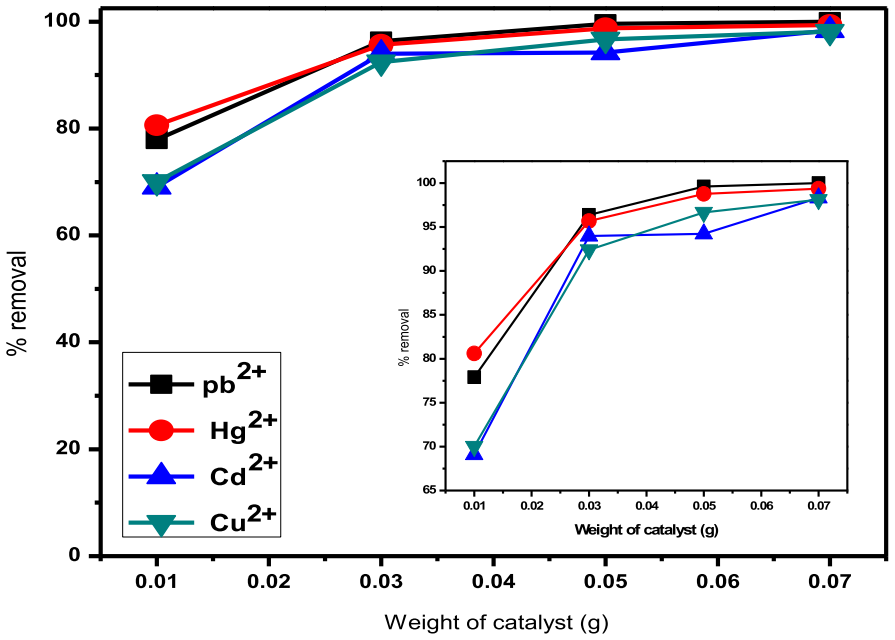

Figure 13. Effect of the weight of the catalyst on the adsorption of Cd^{2+}, Pb^{2+}, Cu^{2+}, and Hg^{2+} after 120 min using 0.03 g of the 50%Fe:50%Co-MOF nanocatalyst.

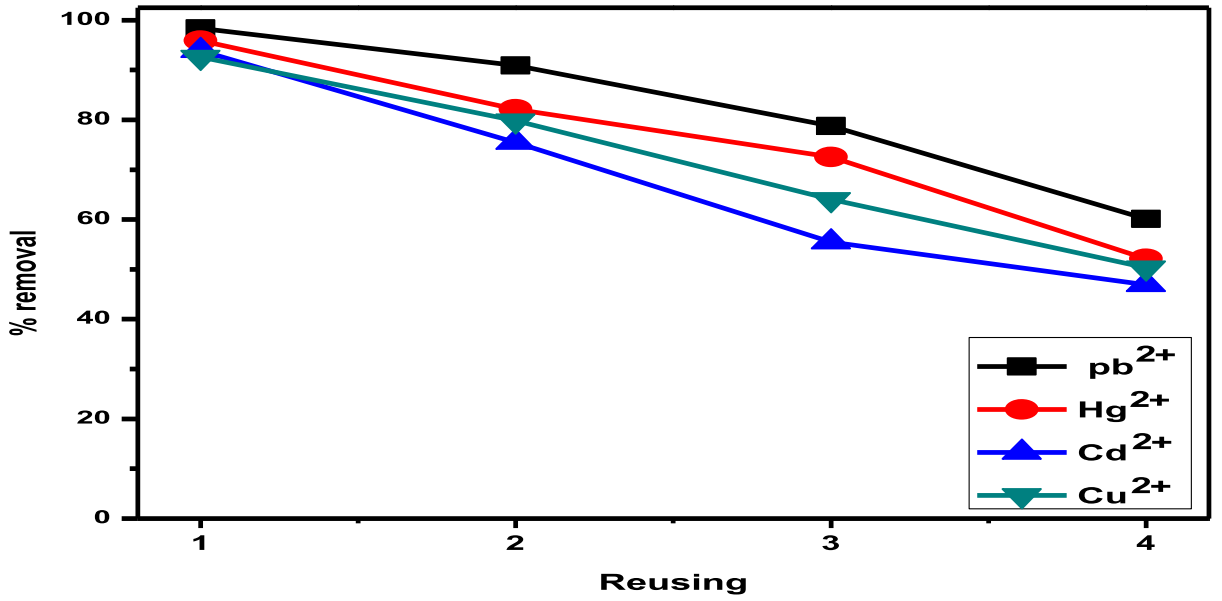

Figure 14. Effect of the reuse of the catalyst on the adsorption of Cd^{2+}, Pb^{2+}, Cu^{2+}, and Hg^{2+} after 120 min using 0.03 g of the 50%Fe:50%Co-MOF nanocatalyst.

can be expressed by a separation factor (R_L), which is defined as

$$R_L = \frac{1}{1 + KC_0} \quad (5)$$

The R_L value implies whether the adsorption is linear (R_L = 1), favorable ($0 < R_L < 1$), unfavorable ($R_L > 1$), or irreversible (R_L = 0). The obtained R_L values were 0.0020, 0.00261, 0.00290, and 0.0035 for lead, mercury, cadmium, and copper cations, respectively, showing that the adsorption of these metal cations on the (Fe/Co) Bi-MOF nanocatalysts was favorable.

K_F and n are Freundlich constants related to adsorption capacity and adsorption intensity, respectively. Generally, $n > 1$ illustrates that the adsorbate is favorably adsorbed on the adsorbent (catalysts), whereas $n < 1$ demonstrates that the adsorption process is chemical in nature. The plot of ln q_e versus ln C_e gave a straight line with a slope of $1/n$ and an intercept of ln K_F. The values found for n were 3.127, 3.097, 1.851, and 2.51 for lead, mercury, cadmium, and copper cations, respectively, which proves that the adsorption of heavy metals on the (Fe/Co) Bi-MOF nanocatalysts is favorable and physical in nature.

The results show that the R^2 values obtained from the Langmuir isotherm for lead, mercury, cadmium, and copper ion adsorption on the (Fe/Co) Bi-MOF nanocatalysts were higher than those obtained from the Freundlich isotherm: the R^2 values from the Langmuir isotherm were 0.9998, 9997,

https://doi.org/10.1021/acsomega.2c01770
ACS Omega 2022, 7, 23421−23444

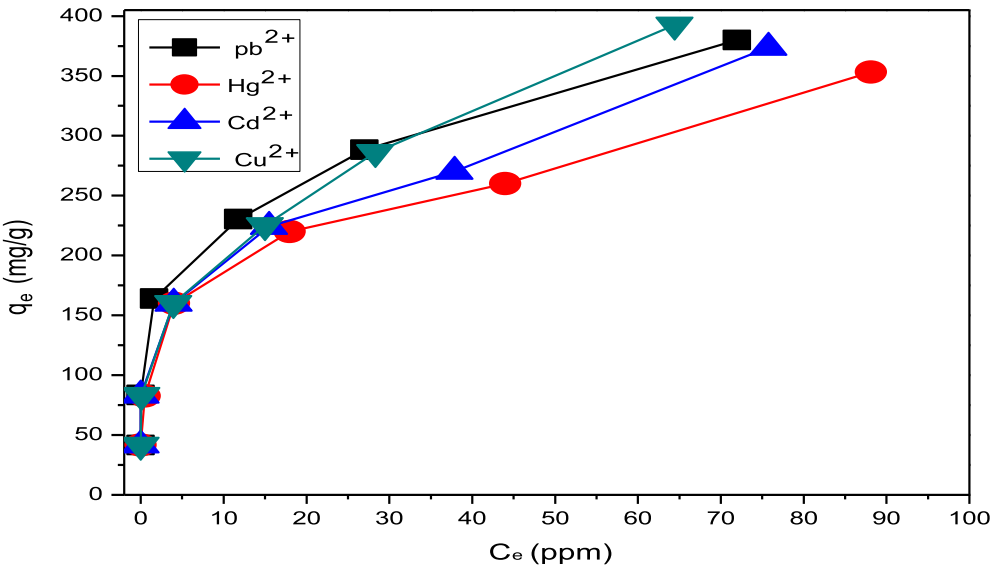

Figure 15. Equilibrium adsorption isotherms of Cd^{2+}, Pb^{2+}, Cu^{2+}, and Hg^{2+} on the 50%Fe:50%Co-MOF nanocatalyst.

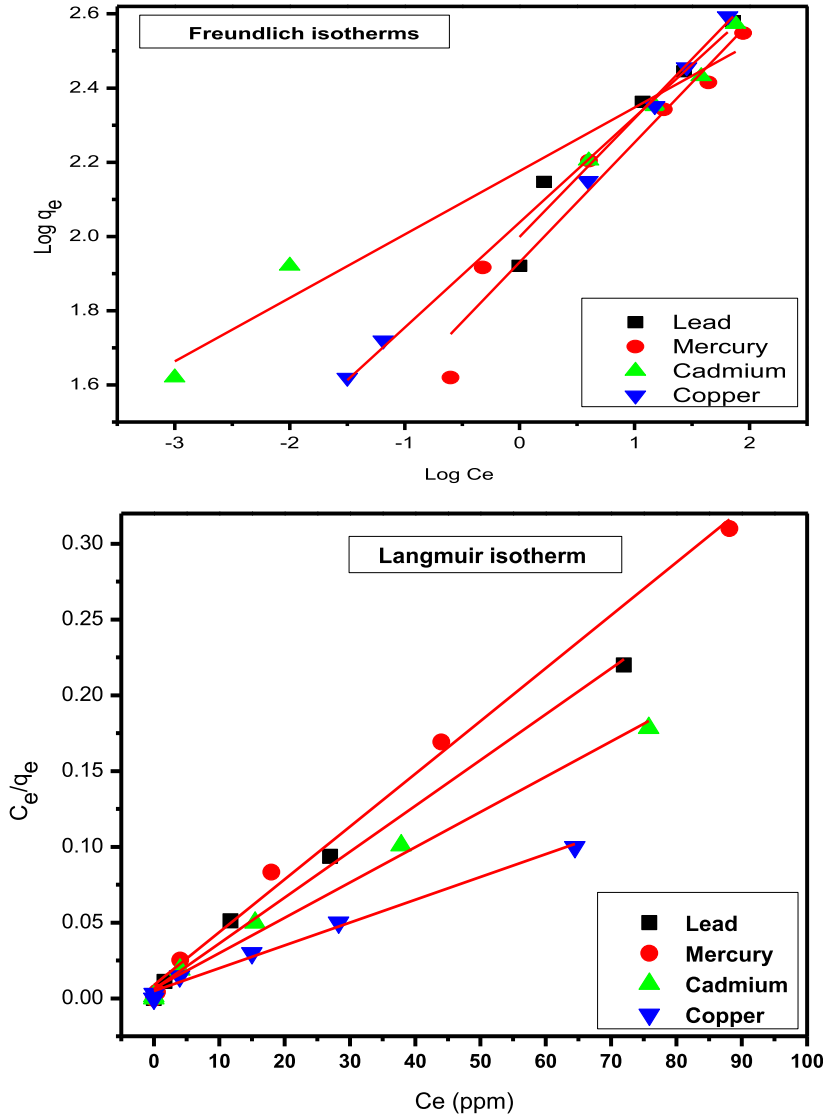

Figure 16. Linear form of Langmuir and Freundlich isotherms for Pb^{2+}, Hg^{2+}, Cd^{2+}, and Cu^{2+} on the 50%Fe:50%Co-MOF nanocatalyst.

https://doi.org/10.1021/acsomega.2c01770
ACS Omega 2022, 7, 23421−23444

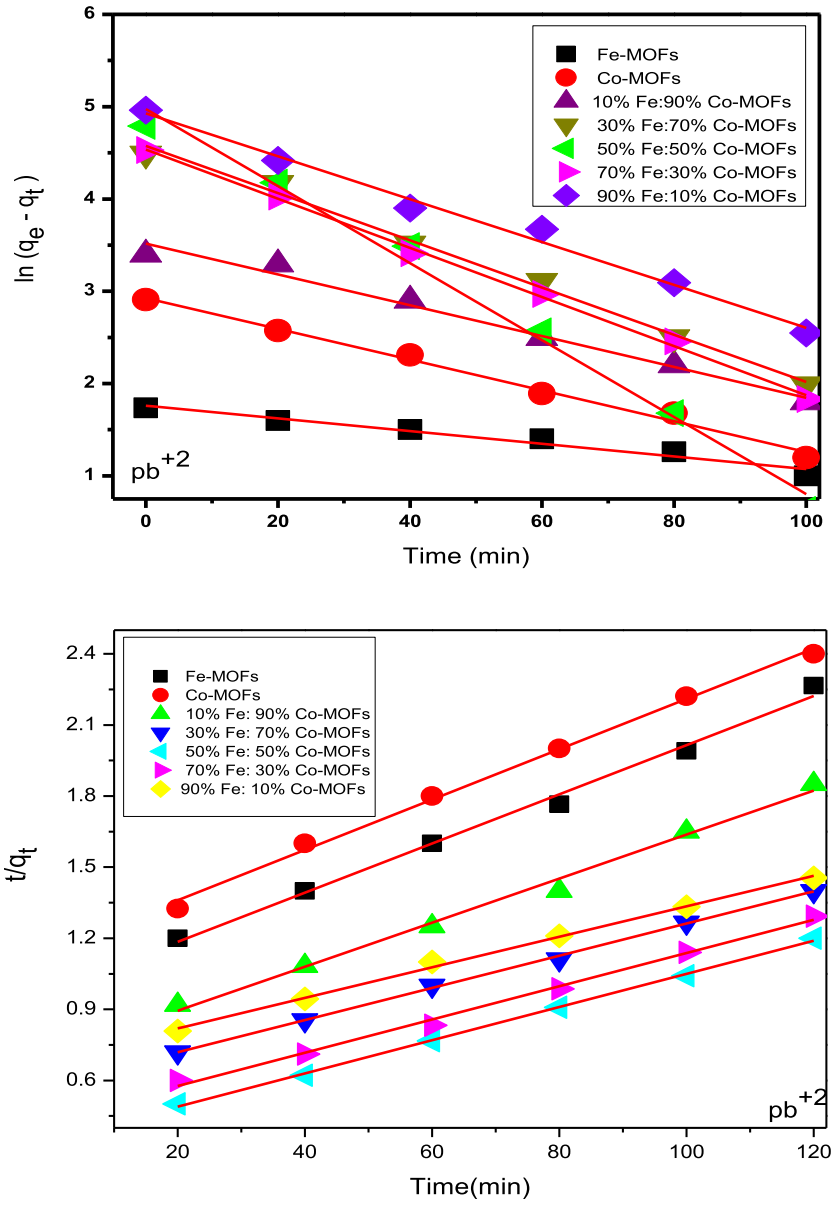

Figure 17. Pseudo-first-order and pseudo-second-order kinetic models for the adsorption of Pb^{2+} by Fe-MOF, Co-MOF, 10%Fe:90%Co-MOF, 30%Fe:70%Co-MOF, 50%Fe:50%Co-MOF, 70%Fe:30%Co-MOF, and 90%Fe:10%Co-MOF samples.

9985, and 0.9978, whereas those from the Freundlich isotherm were 0.9642, 0.9637, 95.71, and 0.9108, respectively. This shows that the adsorption of lead, mercury, cadmium, and copper cations on the (Fe/Co) Bi-MOF nanocatalysts using the Langmuir isotherm model was favorable. The equilibrium adsorption isotherms of lead, mercury, cadmium, and copper cations onto the 50%Fe:50%Co-MOF nanocatalyst are described in Figure 15, whereas the Langmuir and Freundlich isotherms are described in Figure 16.

3.5.7. Kinetic Study. Adsorption kinetics is an important characteristic when determining the pollutant adsorption process efficiency. The adsorption of a solute by solid catalysts in aqueous pollutant solutions is a phenomenon that usually has complex kinetics. In this study, adsorption kinetics describes the rate of adsorbate (heavy metals) uptake onto the (Fe/Co) Bi-MOF catalyst samples. Several kinetic models are available to help us understand the behavior of adsorbents, examine the controlling mechanisms of the adsorption process, and test the experimental data. In the present investigation, the adsorption data were analyzed using two famous kinetic models: the pseudo-first-order model of heavy metal adsorption, which can be expressed by the equation[71]

$$\ln(q_e - q_t) = \ln q_e - k_1 \tag{6}$$

and the pseudo-second-order model of adsorption, which may be written as[72]

$$\frac{t}{q_t} = \frac{1}{k_2 q_e^2} + \frac{t}{q_e} \tag{7}$$

The results confirmed that the pseudo-first-order kinetic model did not produce good linearity, and the predicted q_e values obtained from this kinetic model did not display good agreement with the experimental ones. This suggested that heavy metal adsorption by (Fe/Co) Bi-MOF nanoparticles would not follow the pseudo-first-order kinetic model. Meanwhile, the pseudo-second-order kinetic model produced

https://doi.org/10.1021/acsomega.2c01770
ACS Omega 2022, 7, 23421−23444

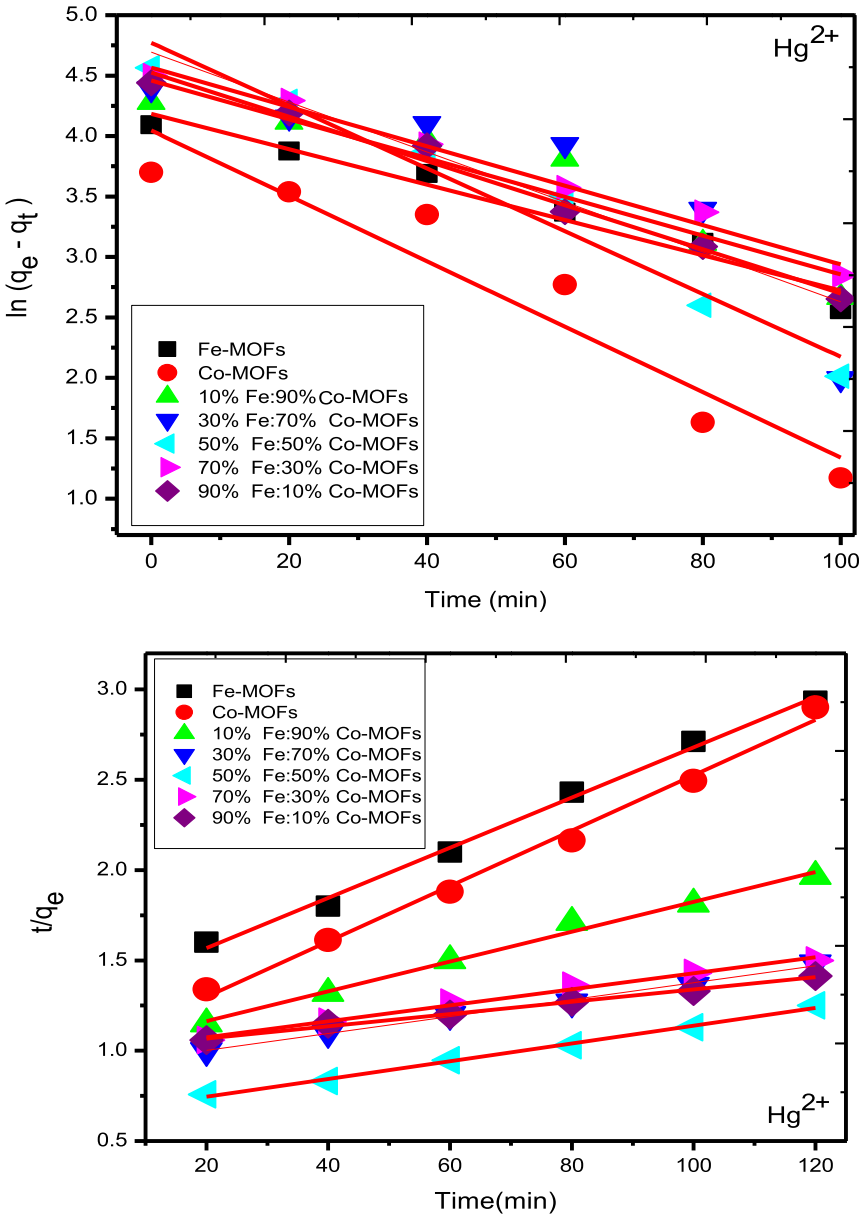

Figure 18. Pseudo-first-order and pseudo-second-order kinetic models for the adsorption of Hg^{2+} by Fe-MOF, Co-MOF, 10%Fe:90%Co-MOF, 30%Fe:70%Co-MOF, 50%Fe:50%Co-MOF, 70%Fe:30%Co-MOF, and 90%Fe:10%Co-MOF samples.

good linearity, and the experimental and calculated q_e values were obtained from this kinetic model as the value of R^2 of the pseudo-second-order kinetic model was higher than that of the pseudo-first-order kinetic model. In addition, the application of the pseudo-first-order model to the kinetic adsorption curves of lead, mercury, cadmium, and copper cations on the (Fe/Co) Bi-MOF nanocatalysts gave q_e values that are significantly lower than the corresponding experimental ones. These suggested that the pseudo-second-order adsorption mechanism for the adsorption of lead, mercury, cadmium, and copper ions on the (Fe/Co) Bi-MOF nanocatalysts was dominant, showing that the adsorption process is controlled by chemisorption (the rate-limiting step in the adsorption of heavy metal ions is chemisorption), which involves valiancy forces through the sharing or exchange of electrons between the solvent and adsorbate.[73] The pseudo-first-order and pseudo-second-order models of heavy metal adsorption are described in Figures 17−20.

3.5.8. Mechanism of Adsorption of Heavy Metals. The infrared spectroscopy technique has proven to be a reliable technique for studying the interaction of a catalyst surface with pollutant species during the adsorption process of inorganic or organic pollutants from aqueous solutions. The change in the intensity of FTIR peaks after the adsorption process of heavy metals can be used to indicate interactions of the heavy metals with functional groups on the (Fe/Co) Bi-MOF nanocatalyst. Thus, FTIR spectra before and after metal ion adsorption were obtained and compared to identify the interaction of the 50% Fe:50%Co-MOF nanocatalyst surface with adsorbed heavy metals (Pb^{2+}, Hg^{2+}, Cd^{2+}, and Cu^{2+}). Figure 21 shows that the intensities of characteristic FTIR peaks of the main M−O, M−OH, C═O, and −C−O groups (as functional groups) were decreased after the adsorption of Pb^{2+}, Hg^{2+}, Cd^{2+}, and Cu^{2+} compared with those of the fresh 50%Fe:50%Co-MOF nanocatalyst, which indicates that these functional groups participated in the adsorption process of Pb^{2+}, Hg^{2+}, Cd^{2+}, and

https://doi.org/10.1021/acsomega.2c01770
ACS Omega 2022, 7, 23421−23444

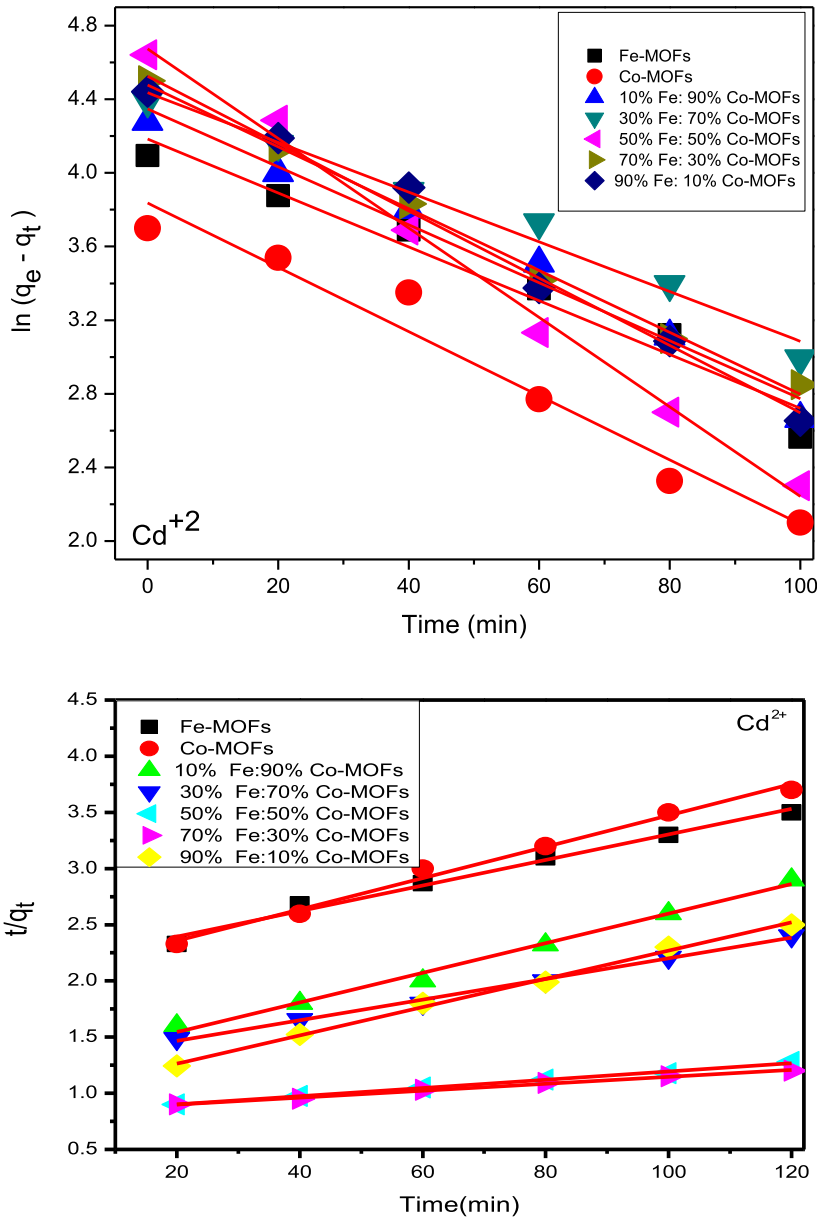

Figure 19. Pseudo-first-order and pseudo-second-order kinetic models for the adsorption of Cd^{2+} by Fe-MOF, Co-MOF, 10%Fe:90%Co-MOF, 30%Fe:70%Co-MOF, 50%Fe:50%Co-MOF, 70%Fe:30%Co-MOF, and 90%Fe:10%Co-MOF samples.

Cu^{2+}. It was seen from the survey FTIR spectrum of the 50% Fe:50%Co-MOF nanocatalyst after the adsorption process that the FTIR peaks did not shift compared with those of the fresh (Fe/Co) Bi-MOF catalyst, indicating that the catalyst structure did not change after the adsorption of Pb^{2+}, Hg^{2+}, Cd^{2+}, and Cu^{2+}, which clearly indicates the presence of the adsorbed metals on the catalyst surface. This result might be related to the chemical interactions between (Fe/Co) Bi-MOFs and the heavy metal ions, as well as related to the formation of van der Waals forces, acid−base interactions, and diffusion on the catalyst surfaces. The magnetic properties of (Fe/Co) Bi-MOFs may lead to an improved adsorption rate. Based on the above discussion, it could be concluded that the main functional groups (M−O, M−OH, C═O, and −C−O groups) were key active sites involved in the adsorption process of Pb^{2+}, Hg^{2+}, Cd^{2+}, and Cu^{2+} from aqueous solutions. The proposed adsorption mechanism on the (Fe/Co) Bi-MOF nanocatalyst has been illustrated in the Graphical Abstract.

3.6. Catalytic Activity. *3.6.1. Surface Acidity (Non-aqueous Titration).* Nonaqueous titration was used to investigate the acidity of surfaces, including the total number of acid sites and acidic strength. According to the nonaqueous titration, the initial electrode potential (E_i) indicates the maximum acid strength of the surface sites, whereas the range where a plateau is reached (meq/g solid) indicates the total number of acid sites. The nonaqueous titration method was conducted using *n*-butyl amine in acetonitrile. The value for the electrode potential in this method is related to the surface acidity of the catalysts, as shown in Figure 22.

3.6.2. Catalysis of the Quinoxaline Synthesis by (Fe/Co) Bi-MOF Nanocatalysts. We studied the catalysis of quinoxaline synthesis at 80 °C in the presence of catalytic amounts of (Fe/Co) Bi-MOF nanocatalysts (0.03 g). The progress of the reaction was monitored using TLC. After the completion of the reaction, the catalysts were filtered off, washed, and dried. The combined organic layers were then washed and dried. The

https://doi.org/10.1021/acsomega.2c01770
ACS Omega 2022, 7, 23421−23444

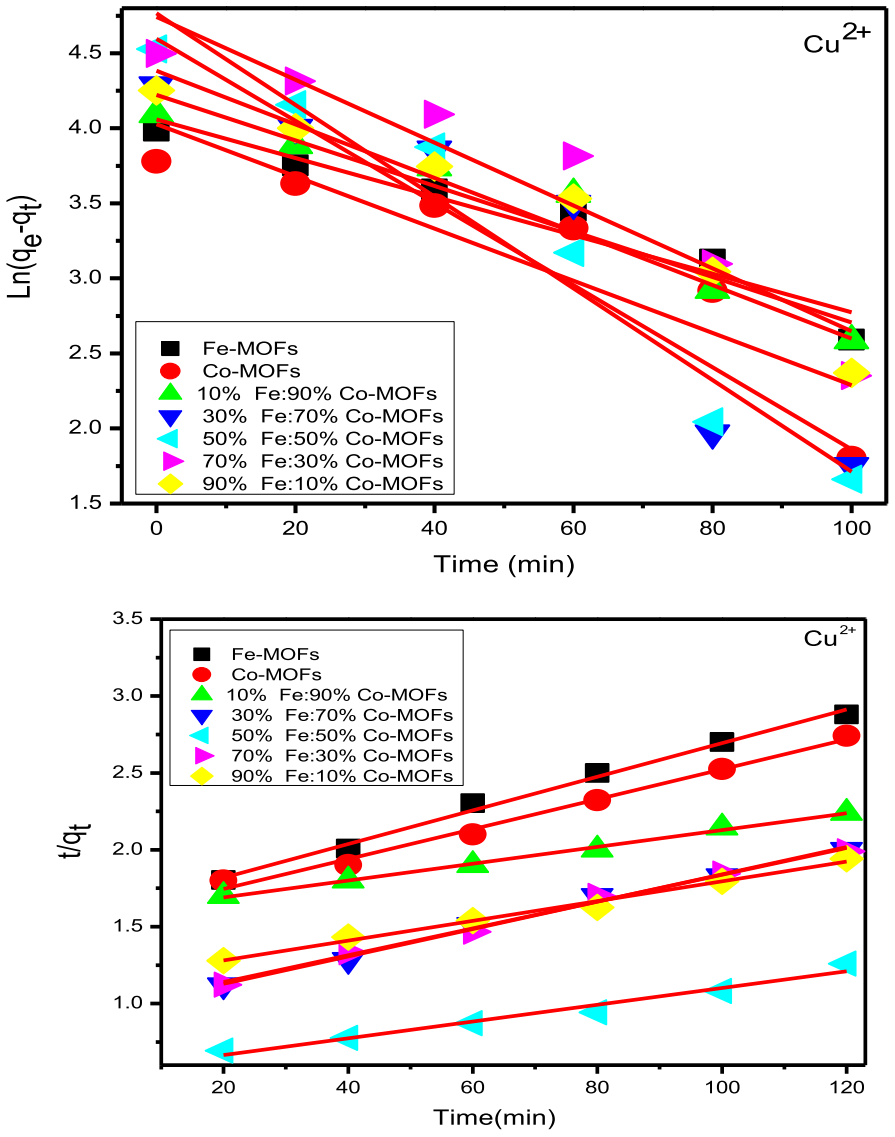

Figure 20. Pseudo-first-order and pseudo-second-order kinetic models for the adsorption of Cu^{2+} by Fe-MOF, Co-MOF, 10%Fe:90%Co-MOF, 30%Fe:70%Co-MOF, 50%Fe:50%Co-MOF, 70%Fe:30%Co-MOF, and 90%Fe:10%Co-MOF samples.

solvent was evaporated under reduced pressure, and pure products were obtained without any further purification.[37,74] Figure 23 shows the FTIR analysis of the quinoxaline compounds. A wide range of homogeneous and heterogamous catalysts such as Cu (BDC), Fe_3O_4, HCl, and iodine are well-suited for such reactions.[54,75−77]

3.6.2.1. Effect of the Percentages of Iron and Cobalt Metals in (Fe/Co) Bi-MOFs on the Catalytic Activity. The effect of the percentages of iron and cobalt in (Fe/Co) Bi-MOFs on catalytic activity was studied using 0.03 g of the different catalysts (Fe-MOF, Co-MOF, 10%Fe:90%Co-MOF, 30%Fe:70%Co-MOF, 50%Fe:50%Co-MOF, 70%Fe:30%Co-MOF, and 90%Fe:10%Co-MOF) for the catalysis of the quinoxaline synthesis. From Figure 24, the quinoxaline yield percentage increased gradually with the increasing percentages of iron up to the maximum at 50%Fe:50%Co-MOF and then decreased. This conforms with the XRD and TEM results, which showed that the nanosize of the (Fe/Co) Bi-MOF catalysts decreased with the increasing percentage of iron up to the maximum at 50%Fe:50%Co-MOF and then increased. When the nanosize decreased, the surface area increased, the number of active sites on the catalyst surface increased, and the catalytic activity was very high.

Figure 25 and Table 1 show that the catalytic activity and number of acid sites increased with the increasing iron percentage up to 50%Fe:50%Co-MOF and then decreased. The increase in the surface acidity may have been due to the strong interaction between the greater amounts of iron in Bi-MOFs and cobalt.

3.6.2.2. Effect of the Molar Ratio of o-Phenylenediamine/Diethyl Oxalate. The molar ratio of reactants in any catalytic reaction is one of the most important parameters that must be optimized.[78] The effect of the molar ratio of *o*-phenylenediamine to diethyl oxalate ranging from 1:1 to 1:5 on the quinoxaline synthesis at 80 °C by the 0.03-g 50%Fe:50%Co-MOF nanocatalyst was investigated. The results are shown in Figure 26. It can be observed that the percentage yield of quinoxaline increased from 93.40 to 95.51 and 98.38% as the molar ratio of *o*-phenylenediamine to diethyl oxalate is increased from 1:1 to 1:2 and 1:3, respectively. Thereafter, the yield percentage decreased from 95.15 to 90.15% with the increase in the molar ratio of *o*-phenylenediamine to diethyl

https://doi.org/10.1021/acsomega.2c01770
ACS Omega 2022, 7, 23421−23444

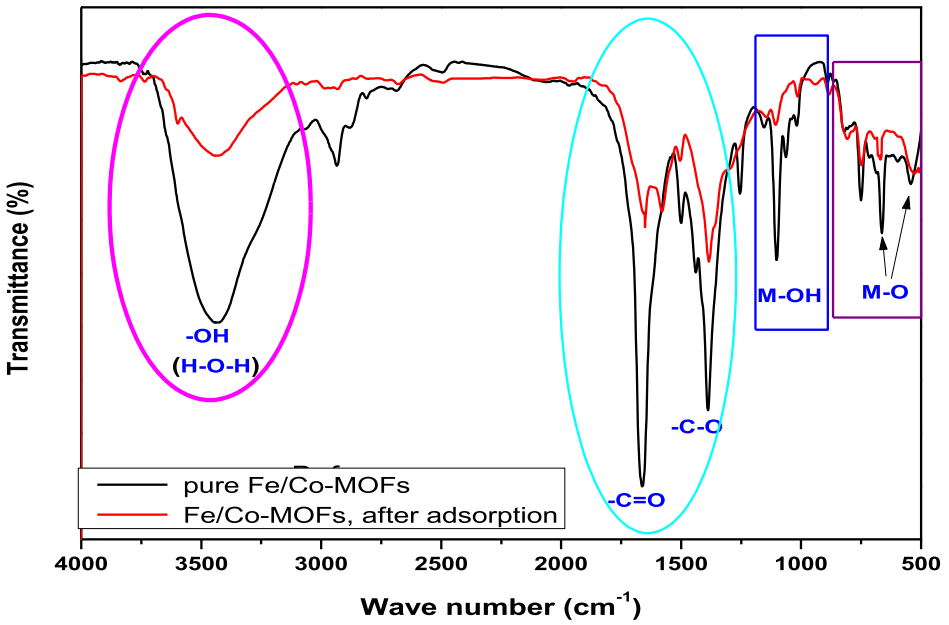

Figure 21. FTIR spectra of 50%Fe:50%Co-MOF before and after the adsorption process.

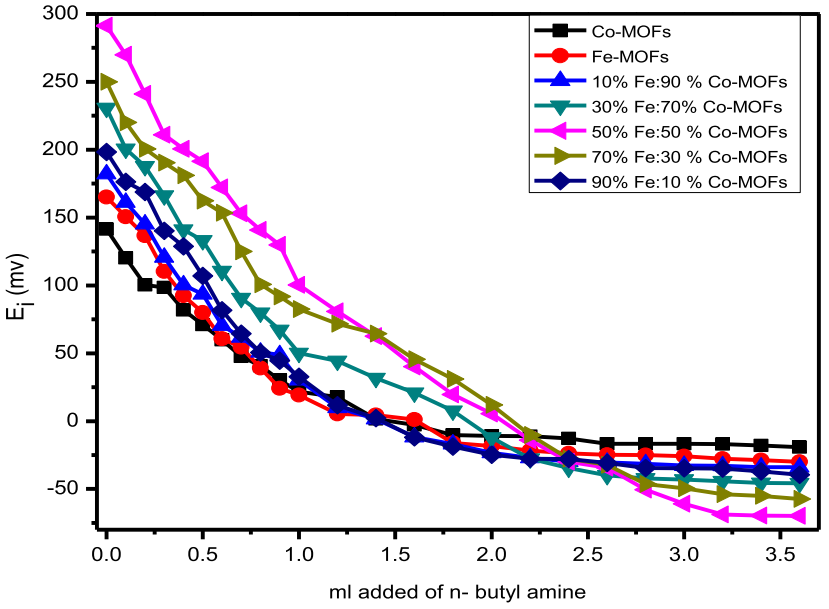

Figure 22. Potentiometric titration curve of *n*-butylamine in acetonitrile for Fe-MOF, Co-MOF, 10%Fe:90%Co-MOF, 30%Fe:70%Co-MOF, 50% Fe:50%Co-MOF, 70%Fe:30%Co-MOF, and 90%Fe:10%Co-MOF samples.

oxalate from 1:4 to 1:5. From these results, the 1:3 m ratio of *o*-phenylenediamine to diethyl oxalate was the optimum for the synthesis of quinoxaline. The decrease in the catalytic activity of the 50%Fe:50%Co-MOF nanocatalyst at molar ratios of 1:4 and 1:5 may be explained on the basis of the fact that the increase in the diethyl oxalate concentration hinders the reaction by blocking active sites on the catalyst surface as a result of the saturation of the active sites with diethyl oxalate molecules.[78,79]

3.6.2.3. Reusability (Recyclability) Study of the Catalysts. The reusability of heterogeneous catalysts is an important aspect of any industrial process. Thus, we studied the reusability of the 50%Fe:50%Co-MOF catalyst by conducting repeated runs of the reaction at 80 °C and keeping the reactant molar ratio of *o*-phenylenediamine to diethyl oxalate at 1:1. The 50%Fe:50%Co-MOF catalyst was regenerated after every 2 h of reaction time, and it was separated through filtration, washed with ethanol and DMF, dried at 120 °C for 2 h, and reused in another reaction under similar conditions. Figure 27 shows the results of reusing the catalyst four times. With the increase in the number of usages of the 50%Fe:50%Co-MOF nanocatalyst, its catalytic activity is slightly decreased from 93.40, 86.10, and 82.40, to 76.80 for the first, second, third, and fourth use, respectively, because of the gradual loss of the catalyst weight during filtration and washing.[80,81]

3.6.2.4. Effect of the Weight of the Catalyst on the Synthesis of Quinoxaline. In this part, the amount of the 50% Fe:50%Co-MOF nanocatalyst was varied to 0.01, 0.03, 0.05, and 0.07 g while keeping the molar ratio of *o*-phenylenediamine to diethyl oxalate at 1:1 and the reaction temperature at

https://doi.org/10.1021/acsomega.2c01770
ACS Omega 2022, 7, 23421−23444

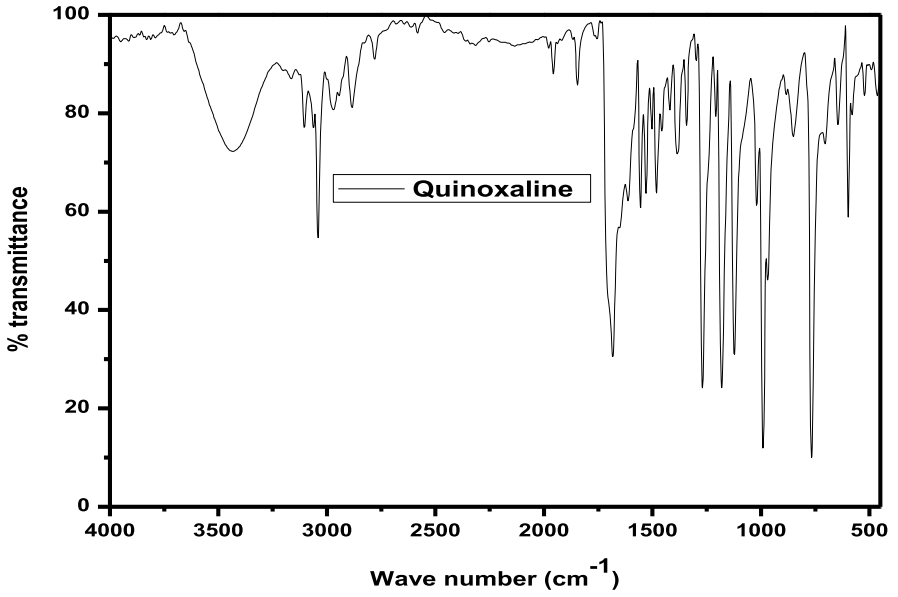

Figure 23. FTIR analysis of the quinoxaline compound.

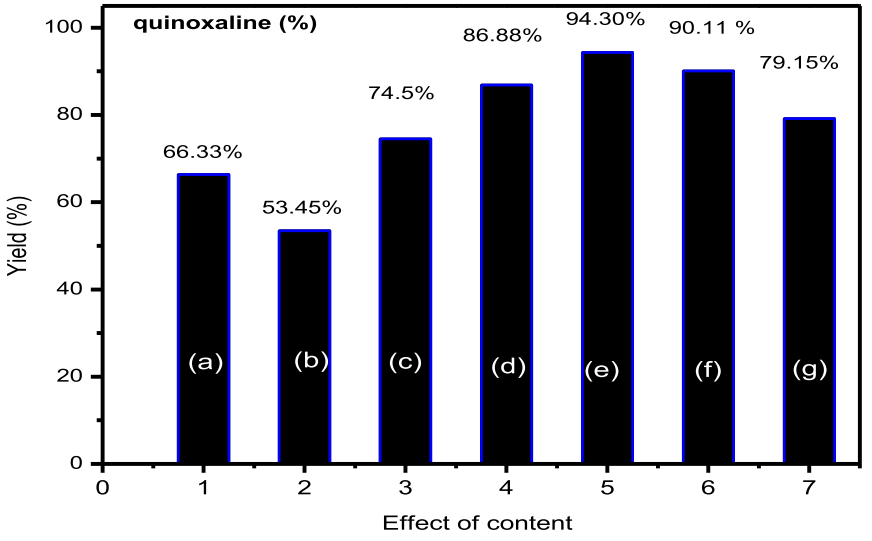

Figure 24. Effect of Fe/Co content on the synthesis of quinoxaline by (a) Fe-MOF, (b) Co-MOF, (c)10%Fe:90%Co-MOF, (d) 30%Fe:70%Co-MOF, (e) 50%Fe:50%Co-MOF, (f) 70%Fe:30%Co-MOF, and (g) 90%Fe:10%Co-MOF samples.

80 °C for 2 h. Figure 28 shows that with the increase in the amount of the 50%Fe:50%Co-MOF nanocatalyst from 0.01, 0.03, and 0.05, to 0.07 g, the quinoxaline yield increased from 71.98, 93.40, and 96.00 to 97.23%, respectively. This was due to the availability of the surface area and acid sites (active sites),[79] where the catalyst weight increased (i.e., the number of nanoparticles increased), increasing the surface area and number of active sites.

3.6.2.5. Effect of the Reaction Time on the Synthesis of Quinoxaline. The influence of the reaction time on the quinoxaline synthesis by the (Fe/Co) Bi-MOF catalysts is given in Figure 29. Using 0.03 g of the 50%Fe:50%Co-MOF nanocomposite as the catalyst under other similar conditions, we studied the effect of various reaction time durations (0.5, 1.0, 1.5, 2.0, and 3.0 h). The results indicate that the quinoxaline yield increased with the increase in reaction time from 0.5 to 2 h. Thereafter, no notable increase or only a slight increase in the quinoxaline yield was observed, suggesting the influence of time on the yield. The percentage yield of quinoxaline increased from 18.00, 49.91, 74.44, and 94.30 to 94.81% after 0.5, 1.0, 1.5, 2.0, and 3.0 h, respectively. This means that the catalyst activity established equilibrium after 2 h.

3.6.2.6. Effect of the Used Solvent in the Reaction. Solvents are known to significantly affect the rates of catalytic activities. The effect of the used solvent is attributed to various factors, which include the solubility of the yield, thermodynamic interaction of the solvent with the reactants and products, and competitive adsorption of the solvent. Different reaction media were used to perform quinoxaline synthesis, such as those using H_2O, C_2H_5OH, DMF, and dimethyl sulfoxide (DMSO) as solvents. Figure 30 clearly shows that under the same reaction conditions, when water and ethanol were used as solvents, the reaction led to relatively higher yields and shorter reaction times; the quinoxaline yields were 93.4 and 92.12% with ethanol and water, respectively.[34,82] In

https://doi.org/10.1021/acsomega.2c01770
ACS Omega 2022, 7, 23421−23444

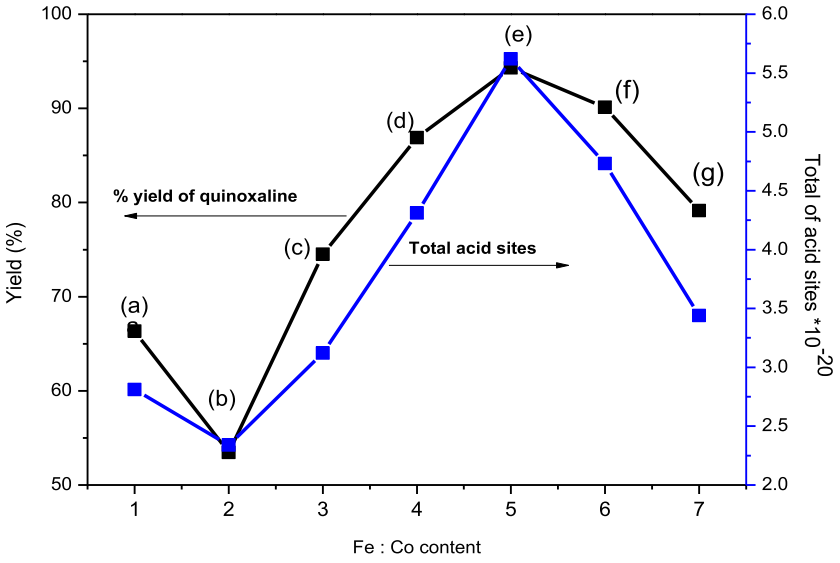

Figure 25. Effect of Fe/Co content and total acid sites on the synthesis of quinoxaline by (a) Fe-MOF, (b) Co-MOF, (c)10%Fe:90%Co-MOF, (d) 30%Fe:70%Co-MOF, (e) 50%Fe:50%Co-MOF, (f) 70%Fe:30%Co-MOF, and (g) 90%Fe:10%Co-MOF samples.

Table 1. Total Number of Acid Sites of the Prepared Samples

sample	E_i (Mv)	no. of acid sites*10^{-20}	quinoxaline (%)	xanthene (%)
Fe-MOF	165.1	2.81	66.32	41.76
Co-MOF	141.4	2.34	53.45	32.5
10%Fe:90%Co-MOF	182.2	3.12	74.50	60.00
30%Fe:70%Co-MOF	230.6	4.31	86.88	78.99
50%Fe:50%Co-MOF	291.2	5.62	94.30	87.45
70%Fe:30%Co-MOF	250.0	4.73	90.11	81.03
90%Fe:10%Co-MOF	198.4	3.44	79.15	73.26

comparison, under the same reaction conditions, when DMF and DMSO were used as solvents, the yield decreased to 71.71 and 45.03%, respectively. This decrease in the yield may have been caused by the solvent dissolving the formed yield.[34,83]

3.6.3. Catalysis of the Dibenzoxanthene Synthesis via (Fe/Co) Bi-MOF Catalysts. We studied the catalysis of dibenzoxanthene synthesis at 70 °C in the presence of a catalytic amount of (Fe/Co) Bi-MOF nanocatalysts (0.03 g). The progress of the reaction was monitored using TLC. After the completion of the reaction, the catalyst was filtered off, washed, and dried. The combined organic layers were then washed and dried. The solvent was evaporated under reduced pressure, and a pure product was obtained without any further purification.[37,74] Figure 31 shows the FTIR analysis of the dibenzoxanthene compound.

3.6.3.1. Effect of the Percentages of Iron and Cobalt in (Fe/Co)-MOFs on the Catalytic Activity. The effect of the percentages of iron and cobalt in Bi-MOFs on catalytic activity using 0.03 g of different (Fe/Co) Bi-MOF catalysts for the catalysis of dibenzoxanthene synthesis processes was also studied. As shown in Figure 32, the percentage of

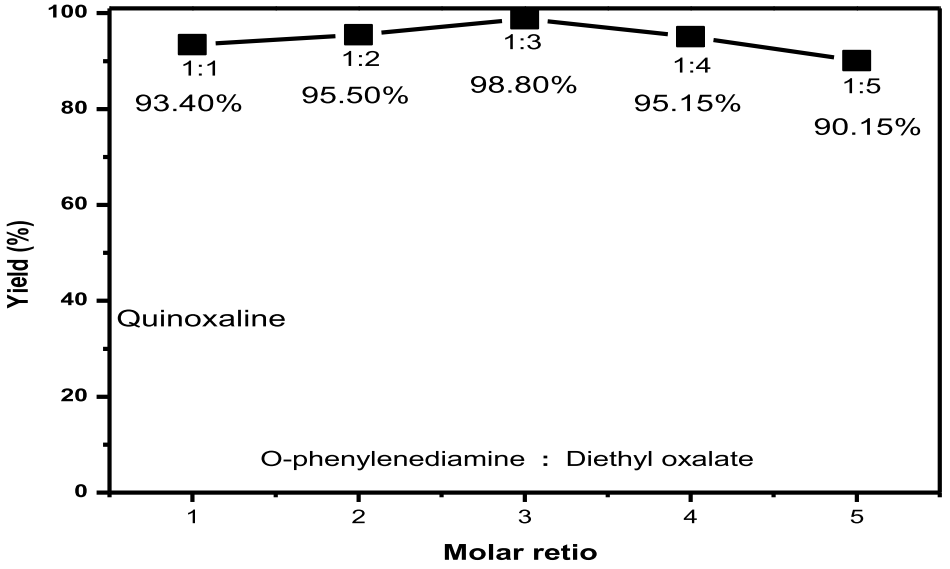

Figure 26. Effect of the molar ratio of *o*-phenylenediamine: diethyl oxalate on the synthesis of quinoxaline by the 50%Fe:50%Co-MOF nanocatalyst.

https://doi.org/10.1021/acsomega.2c01770
ACS Omega 2022, 7, 23421−23444

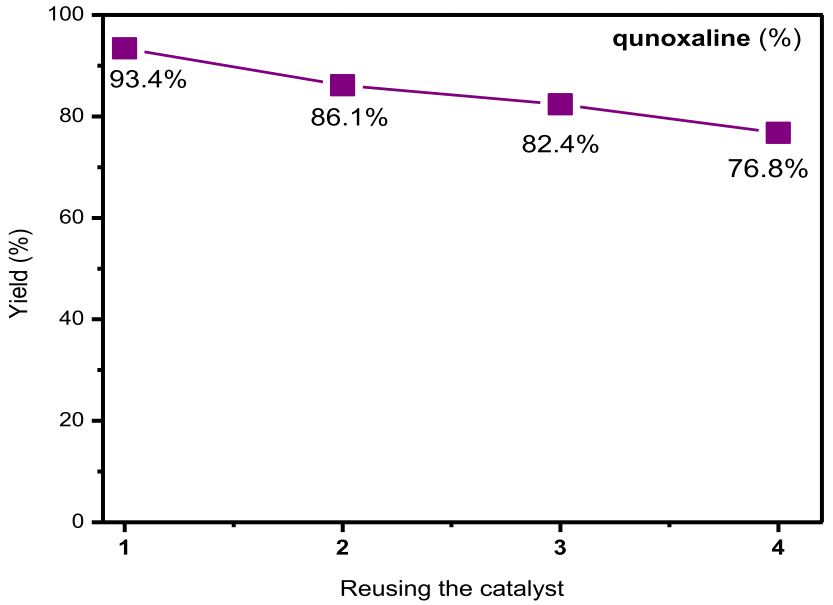

Figure 27. Effect of reusing the prepared catalysts on the synthesis of quinoxaline using 0.03 g of the 50%Fe:50%Co-MOF nanocatalyst.

dibenzoxanthene yield increased gradually with the increase in the percentage of iron up to 50%Fe:50%Co-MOF and then decreased. This conforms with the XRD and TEM results, which showed that the nanosize of the (Fe/Co) Bi-MOF catalysts decreases with the increase in the percentage of iron up to 50%Fe:50%Co-MOF and then decreased. As the nanosize decreased, the surface area increased, the number of active sites on the catalyst surface increased, and thus, the catalytic activity is increased.[84]

From Figure 33 and Table 1, the catalytic activity and the number of acid sites increased with the increase in iron percentage to 50%Fe:50%Co-MOF and then decreased. The increase in the surface acidity may have been due to the strong interaction between the greater amounts of iron in Bi-MOFs and cobalt.

3.6.3.2. Effect of the Molar Ratio of β-Naphthol/Benzaldehdyde. We studied the effect of the molar ratio of β-naphthol to benzaldehyde (from 2:1 to 2:5) on the synthesis of dibenzoxanthene at 70 °C using 0.03 g of the 50%Fe:50% Co-MOF catalyst. Figure 34 shows that the percentage yield of dibenzoxanthene increased from 73.11 and 85.20 to 87.04% with the increase in the molar ratio of β-naphthol to benzaldehyde from 2:1 and 2:2 to 2:3, respectively. Therefore, the yield percentage increased with the increase in the molar ratio of β-naphthol to benzaldehyde from 2:4 to 2:5. From these results, the molar ratio of 2:3 was found to be optimum for the synthesis of dibenzoxanthene. The absence of an increase in the catalytic activity of the 50%Fe:50%Co-MOF nanocatalyst at molar ratios of 1:3 to 1:4 may have been because β-naphthol was completely consumed in the reaction. Thus, both the benzaldehyde concentration and the amount of β-naphthol must be increased in the reaction.

3.6.3.3. Reusability (Recyclability) Study of the Catalysts. We also studied the reusability of the prepared nanocatalysts while keeping the reactant molar ratio of β-naphthol to benzaldehyde at 2:3. Figure 35 shows the result of reusing the catalysts four times. The catalytic activity of the 50%Fe:50% Co-MOF catalyst is slightly decreased from 87.45, 78.81, and 73.29 to 66.59 for the first, second, third, and fourth use, respectively, because of the gradual loss of the catalyst weight during filtration and washing.[17,81] The 50%Fe:50%Co-MOFs catalyst was regenerated after every 30 min of reaction time, and it was separated through filtration, washed with ethanol and DMF, dried at 70 °C for 30 min, and reused in other reactions under similar conditions.

3.6.3.4. Effect of the Weight of the Catalyst on the Synthesis of Dibenzoxanthene. The amount of the 50% Fe:50%Co-MOF nanocatalyst was varied from 0.01, 0.03, and 0.05, to 0.8 g while keeping the molar ratio of β-naphthol to benzaldehyde at 2:3 and the reaction temperature at 70 °C for 30 min. Figure 36 indicates that with the increase in the amount of the 50%Fe:50%Co-MOF nanocatalyst from 0.01, 0.03, and 0.05 to 0.08 g, the yield of dibenzoxanthene increased from 70.66, 87.45, and 89.98 to 92.33%, respectively. This is due to the availability of the surface area and acid sites (active sites).[67] As the catalyst weight increased (i.e., the number of nanoparticles increased), the surface area and number of active sites increased.

3.6.3.5. Effect of the Reaction Time on the Synthesis of Dibenzoxanthene. We studied the influence of the reaction time on the synthesis of dibenzoxanthene by (Fe/Co) Bi-MOF nanocatalysts. In this regard, 0.03 g of 50%Fe:50%Co was taken as the catalyst under other similar conditions. Figure 37 shows the effect of 10, 20, 30, and 40 min reaction times. The results indicate that the yield of dibenzoxanthene increased with the increase in the reaction time from 10 to 30 min. Thereafter, no notable increase or only a slight increase in the yield of dibenzoxanthene was observed, suggesting the influence of time on the yield. The yield percentage of dibenzoxanthene increased from 25.98, 59.77, and 87.45 to 88.01% after 10, 20, 30, and 40 min, respectively. This means that the catalyst activity established the equilibrium after 30 min.

3.7. Antibacterial and Antioxidant Activities. *3.7.1. Antibacterial Activity.* We study the antibacterial activity and antioxidant activity using MOF and (Fe/Co) Bi-MOF catalysts, where the antibacterial activity of catalysts prepared were individually tested against a panel of Gram-positive *B. subtilis*, Gram-negative *E. coli* bacteria, and *Candida albicans*. Fe-MOF, Co-MOF, and (Fe/Co) Bi-MOF (10%

https://doi.org/10.1021/acsomega.2c01770
ACS Omega 2022, 7, 23421−23444

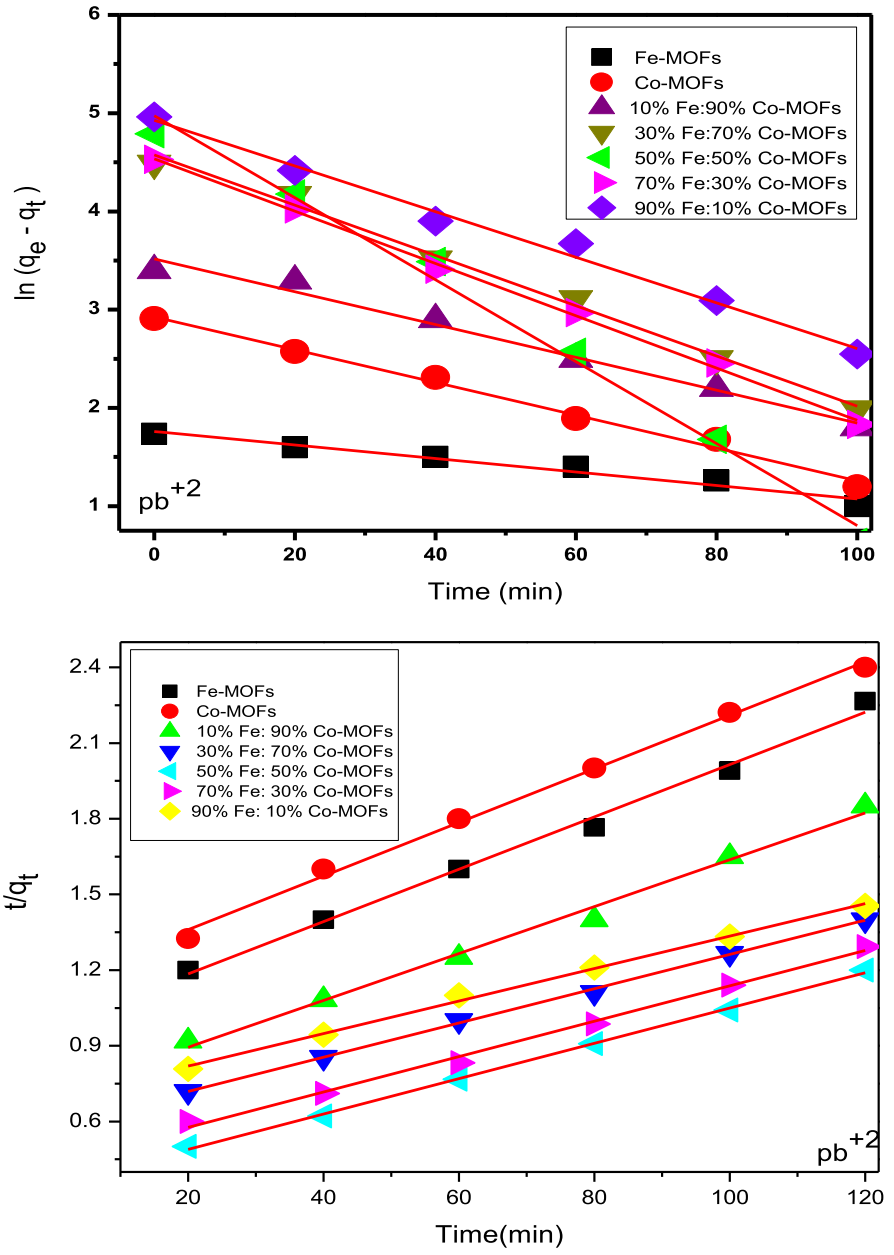

Figure 28. Effect of the weight of the catalyst on the synthesis of quinoxaline by the 50%Fe:50%Co-MOF nanocatalyst.

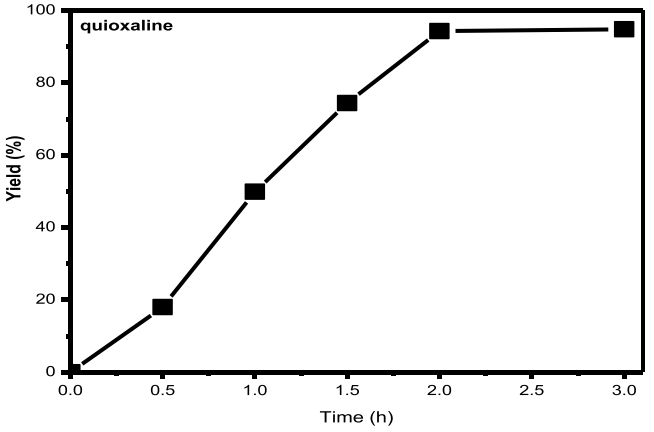

Figure 29. Effect of the reaction time on the synthesis of quinoxaline using 0.03 g of the 50%Fe:50%Co-MOFnanocatalyst.

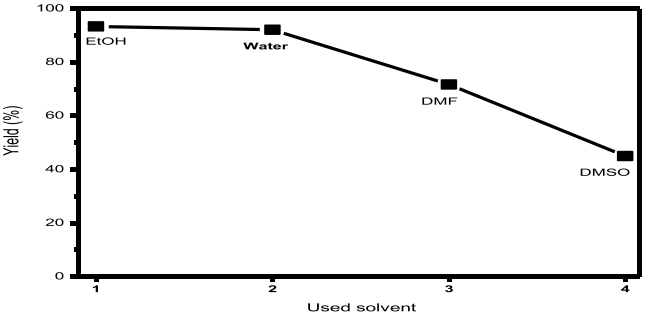

Figure 30. Effect of the used solvent on the synthesis of quinoxaline using 0.03 g of the 50%Fe:50%Co-MOF nanocatalyst.

Fe:90%Co-MOF, 30%Fe:70%Co-MOF, 50%Fe:50%Co-MOF, 70%Fe:30%Co-MOF, and 90% Fe:10%Co-MOF) samples exhibited a remarkable antibacterial activity against the tested

https://doi.org/10.1021/acsomega.2c01770
ACS Omega 2022, 7, 23421−23444

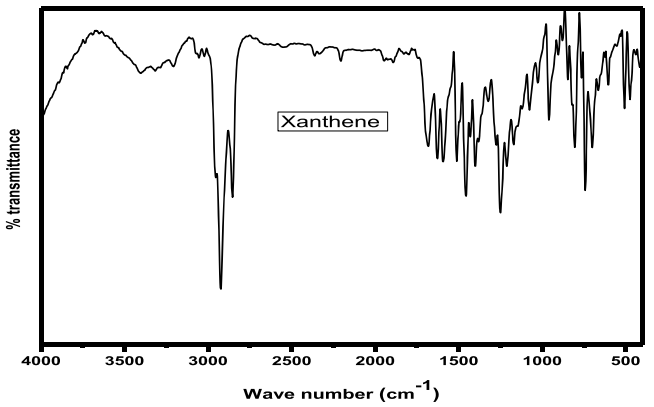

Figure 31. FTIR analysis of the dibenzoxanthene compound.

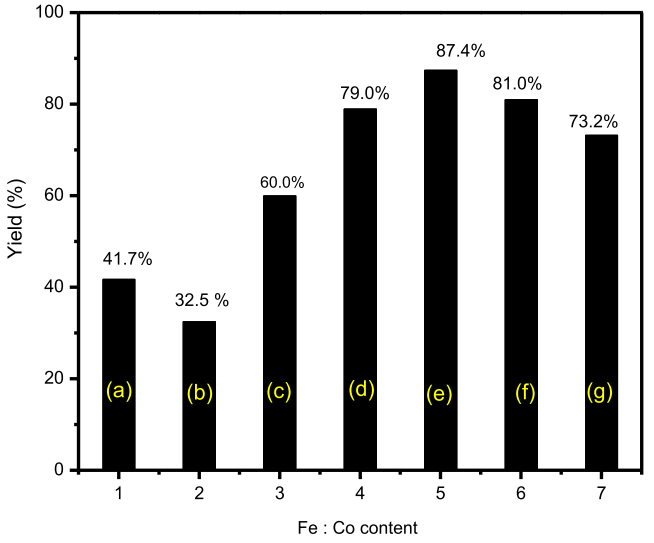

Figure 32. Effect of Fe/Co content on the dibenzoxanthene synthesis by (a) Fe-MOF, (b) Co-MOF, (c)10%Fe:90%Co-MOF, (d) 30% Fe:70%Co-MOF, (e) 50%Fe:50%Co-MOF, (f) 70%Fe:30%Co-MOF, and (g) 90%Fe:10%Co-MOF samples.

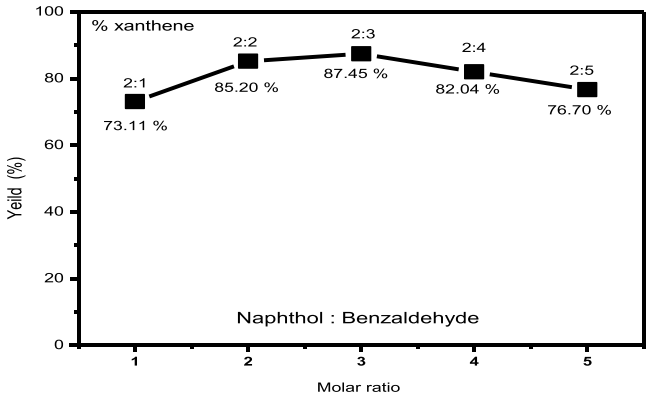

Figure 34. Effect of the molar ratio (β-naphthol: benzaldehyde) on the synthesis of dibenzoxanthene using 0.03 g of the 50%Fe:50%Co-MOF nanocatalyst.

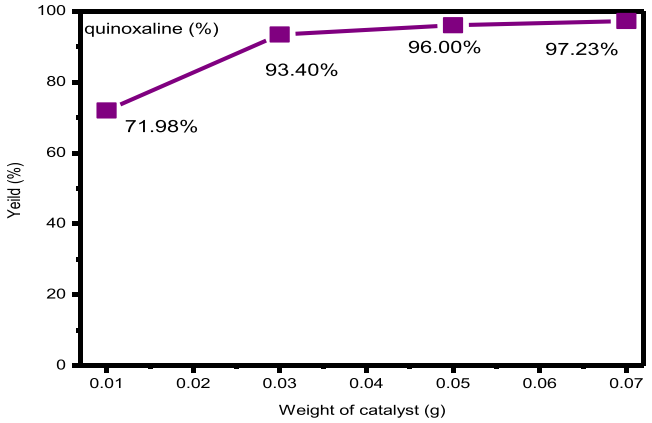

Figure 35. Effect of reusing the catalyst on the synthesis of dibenzoxanthene using 0.03 g of the 50%Fe:50%Co-MOF nanocatalyst.

bacterial strains, as shown in Table 2. The results show that the 50%Fe:50%Co-MOF nanocatalyst exhibited the highest antibacterial activity. The antibacterial activities of the

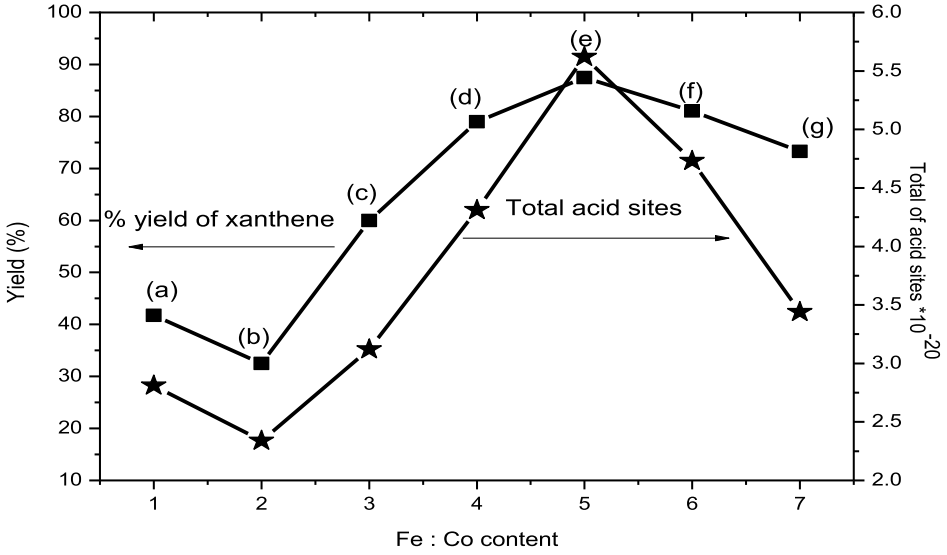

Figure 33. Effect of Fe/Co content and total acid sites on the synthesis of dibenzoxanthene by (a) Fe-MOF, (b) Co-MOF, (c)10%Fe:90%Co-MOF, (d) 30%Fe:70%Co-MOF, (e) 50%Fe:50%Co-MOF, (f) 70%Fe:30%Co-MOF, and (g) 90%Fe:10%Co-MOF samples.

https://doi.org/10.1021/acsomega.2c01770
ACS Omega 2022, 7, 23421−23444

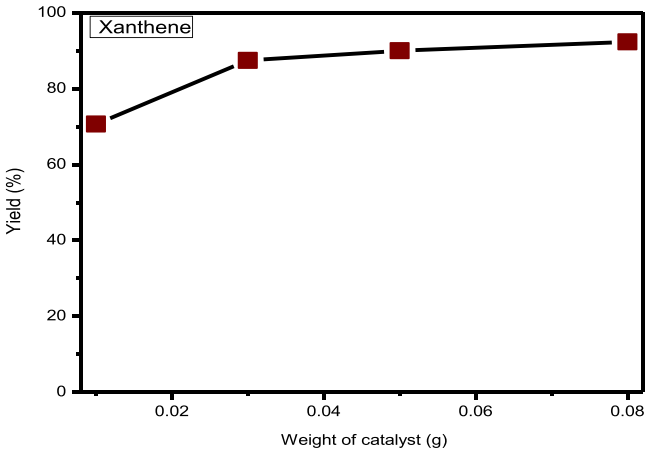

Figure 36. Effect of the weight of the catalyst on the synthesis of dibenzoxanthene by the 50%Fe:50%Co-MOF nanocatalyst.

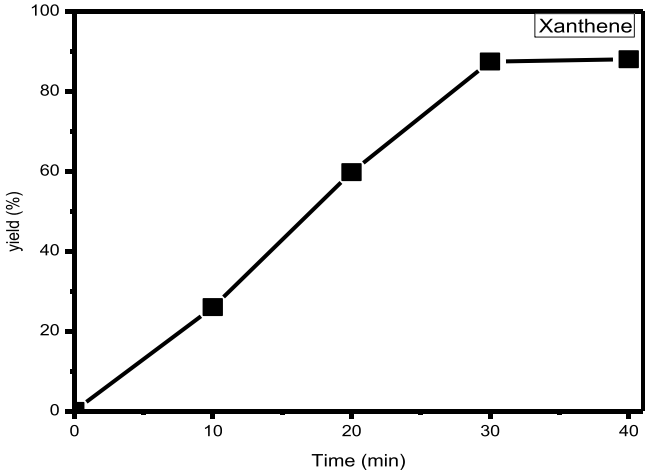

Figure 37. Effect of the reaction time on the synthesis of dibenzoxanthene using 0.03 g of the 50%Fe:50%Co-MOF nanocatalyst.

common standard antibiotic ampicillin and antifungal clotrimazole were also recorded using the same procedure at the same concentration and solvents to be considered as the reference drug.

The % activity index was calculated using the following formula

$$\%\ \text{activity index} = \frac{\text{zone of inhibition by test compound (diametre)}}{\text{zone of inhibition by standard (diametre)} \times 100} \quad (8)$$

3.7.2. Antioxidant Activity. Antioxidant activity of MOF and (Fe/Co) Bi-MOF samples was screened using the ABTS assay method. For each of the investigated compounds (2 mL), ABTS solution (60 μM) was added to 3 mL of MnO_2 solution (25 mg/mL). Fe-MOF and (Fe/Co) Bi-MOF (10%Fe:90% Co-MOF, 30%Fe:70%Co--MOF, 50%Fe:50 % Co)-MOF, 70% Fe:30%Co-MOF, and 90%Fe:10%Co-MOF) samples exhibited a remarkable antioxidant activity, the absorbance was measured, and the reduction in color intensity was expressed as the inhibition percentage, as shown in Table 3. The results show that the 50%Fe:50%Co-MOF sample exhibited the highest antioxidant activity.

Table 3. Antioxidant Activity of the Prepared Samples

method	BTS $Abs_{(control)} - Abs_{(test)}/Abs_{(control)} \times 100$	
compounds	absorbance of samples	% inhibition
control of ABTS	0.510	0%
ascorbic-acid	0.056	89.0%
Co-MOF	41.4%	0.299
Fe-MOF	46.5%	0.273
10%Fe:90%Co-MOF	45.2%	0.279
30%Fe:70%Co-MOF	58.4%	0.212
50%Fe:50%Co-MOF	64.5%	0.181
70%Fe:30%Co-MOF	60.6%	0.201
90%Fe:10%Co-MOF	48.6%	0.262

3.8. Conclusions. (Fe/CO) Bi-MOF nanocatalysts have been successfully attained, obtaining a mixed-metal (Fe/Co) Bi-MOF material series with different weight ratios of Fe and Co. XRD, TEM, SEM and FTIR spectroscopy were used for the characterization of the prepared nanocatalysts. XRD, TEM, and SEM proved that (Fe/Co) Bi-MOFs were obtained with sizes in the nanoscale reaching 3 nm, and FTIR results confirmed that (Fe/Co) Bi-MOFs were formed. The (Fe/Co) Bi-MOFs as good adsorbents showed efficient removal of the toxic heavy metal cationic pollutants (Pb^{2+}, Hg^{2+}, Cd^{2+}, and Cu^{2+}) from the aqueous solution with high adsorption capacity. The nanoscale (Fe/Co) Bi-MOF nanocatalysts as efficient heterogeneous solid acid catalysts showed high catalytic activity with excellent yields and short reaction time in the catalytic reactions of quinoxaline and dibenzoxanthene

Table 2. Antibacterial Activity of the Prepared Catalysts

	C. Albicans (mg/mL)		*B. subtilis* (mg/mL)		*E. coli* (mg/mL)	
catalyst samples	diameter of the inhibition zone (in mm)	% activity index	diameter of the inhibition zone (in mm)	% activity index	diameter of the inhibition zone (in mm)	% activity index
Co-MOF	6	27.3	8	34.8	8	32.0
Fe-MOF	8	36.4	10	43.5	10	40.0
10%Fe:90%Co-MOF	10	45.4	9	40.9	14	56.0
30%Fe:70%Co-MOF	9	40.1	10	43.5	18	72.0
50%Fe:50%Co-MOF	15	68.2	13	56.5	21	84.0
70%Fe:30%Co-MOF	13	59.1	11	47.8	19	76.0
90%Fe:10%Co-MOF	11	50.0	10	43.5	12	48.0
ampicillin	22	100	23	100	no activity	
clotrimazole	no activity		no activity		25	100

https://doi.org/10.1021/acsomega.2c01770
ACS Omega 2022, 7, 23421−23444

compounds. The analysis and experimental results confirmed that the 50%Fe/50%Co-MOF nanocatalyst was the best sample in terms of the adsorption and catalytic activity.

■ ASSOCIATED CONTENT

Supporting Information

The Supporting Information is available free of charge at https://pubs.acs.org/doi/10.1021/acsomega.2c01770.

Highlights of the study (PDF)

■ AUTHOR INFORMATION

Corresponding Author

Fares T. Alshorifi − *Department of Chemistry, Faculty of Science, Sana'a University, Sana'a 15452, Yemen; Department of Chemistry, Faculty of Science, Mansoura University, Mansoura 0020, Egypt;* orcid.org/0000-0002-2818-9613; Phone: 0096777130904; Email: amgdfaress@gmail.com

Authors

Shady M. El Dafrawy − *Department of Chemistry, Faculty of Science, Mansoura University, Mansoura 0020, Egypt*

Awad I. Ahmed − *Department of Chemistry, Faculty of Science, Mansoura University, Mansoura 0020, Egypt*

Complete contact information is available at: https://pubs.acs.org/10.1021/acsomega.2c01770

Notes

The authors declare no competing financial interest.

■ REFERENCES

(1) Tan, K.; Tan, N.; Nijem, N.; Canepa, P.; Gong, Q.; Li, J.; Thonhauser, T.; Chabal, Y. J. Stability and hydrolyzation of metal organic frameworks with paddle-wheel SBUs upon hydration. *J. Am. Chem. Soc.* **2012**, *24*, 3153−3167.

(2) Katzenmeyer, A. M.; Canivet, J.; Holland, G.; Farrusseng, D.; Centrone, A. Assessing chemical heterogeneity at the nanoscale in mixed-ligand metal-organic frameworks with the PTIR technique. *Angew. Chem., Int. Ed.* **2014**, *53*, 2852−2856.

(3) El-Hakam, S. A.; Samra, S. E.; El-Dafrawy, S. M.; Ibrahim, A. A.; Salama, R. S.; Ahmed, A. I. Synthesis of sulfamic acid supported on Cr-MIL-101 as a heterogeneous acid catalyst and efficient adsorbent for methyl orange dye. *RSC Adv.* **2018**, *8*, 20517−20533.

(4) Jeazet, H.; Koschine, T.; Staudt, C.; Raetzke, K.; Janiak, C. Correlation of gas permeability in a metal-organic framework MIL-101(Cr)-polysulfone mixed-matrix membrane with free volume measurements by positron annihilation lifetime spectroscopy (PALS). *Membranes* **2013**, *3*, 331−353.

(5) Ford, D. C.; Dubbeldam, D.; Snurr, R. Q. The effect of framework flexibility on diffusion of small molecules in the metal-organic framework IRMOF-1. *Diffusion Fundamentals* **2009**, *78*, 1−8.

(6) Song, X.; Oh, M.; Lah, M. S. Hybrid bimetallic metal-organic frameworks: modulation of the framework stability and ultralarge CO_2 uptake capacity. *Inorg. Chem.* **2013**, *52*, 10869−10876.

(7) Villajos, J. A.; Orcajo, G.; Martos, C.; Botas, J. Á.; Villacañas, J.; Calleja, G. Co/Ni mixed-metal sited MOF-74 material as hydrogen adsorbent. *Int. J. Hydrogen Energy* **2015**, *40*, 5346−5352.

(8) Kettner, F.; Worch, C.; Moellmer, J.; Gläser, R.; Staudt, R.; Krautscheid, H. Synthesis, crystal structure and catalytic behavior of homo- and heteronuclear coordination polymers [M (tdc)(bpy)] (M^{2+} = Fe^{2+}, Co^{2+}, Zn^{2+}, Cd^{2+}; tdc^{2-} = 2,5-thiophenedicarboxylate). *Inorg. Chem.* **2013**, *52*, 8738−8742.

(9) Brozek, C. K.; Dincă, M. Ti^{3+}-, $V^{2+/3+}$-, $Cr^{2+/3+}$-, Mn^{2+}-, and Fe^{2+}-substituted MOF-5 and redox reactivity in Cr- and Fe-MOF-5. *J. Am. Chem. Soc.* **2013**, *135*, 12886−12891.

(10) Calleja, G.; Sanz, R.; Orcajo, G.; Briones, D.; Leo, P.; Martínez, F. Copper-based MOF-74 material as effective acid catalyst in friedel-crafts acylation of anisole. *Catal. Today* **2014**, *227*, 130−137.

(11) Almáši, M.; Zeleňák, V.; Opanasenko, M.; Císařová, I. Ce(III) and Lu(III) metal−organic frameworks with Lewis acid metal sites: Preparation, sorption properties and catalytic activity in Knoevenagel condensation. *Catal. Today* **2015**, *243*, 184−194.

(12) Cele, M. N.; Friedrich, H. B.; Bala, M. D. Liquid phase oxidation of n-octane to C8 oxygenates over modified Fe-MOF-5 catalysts. *Catal. Commun.* **2014**, *57*, 99−102.

(13) Lotfi, R.; Saboohi, Y. Effect of metal doping, boron substitution and functional groups on hydrogen adsorption of MOF-5: ADFT-D study. *Int. J. Comput. Theor. Chem.* **2014**, *1044*, 36−43.

(14) Zhang, C.; Wang, M.; Liu, L.; Yang, X.; Xu, X. Electrochemical investigation of a new Cu-MOF and its electrocatalytic activity towards H_2O_2 oxidation in alkaline solution. *Electrochem. Commun.* **2013**, *33*, 131−134.

(15) Juan-Alcañiz, J.; Gascon, J.; Kapteijn, F. Metal−organic frameworks as scaffolds for the encapsulation of active species: state of the art and future perspectives. *J. Mater. Chem.* **2012**, *22*, 10102−10118.

(16) Bosch, M.; Zhang, M.; Zhou, H. C. Increasing the stability of metal-organic frameworks. *Adv. Chem.* **2014**, *2014*, 182327.

(17) Tella, A. C.; Aaron, I. Y. Synthesis and application of metal-organic frameworks: a review. *Acta Chim. Pharm. Indica* **2012**, *2*, 75−81.

(18) Villajos, J. A.; Orcajo, G.; Martos, C.; Botas, J. Á.; Villacañas, J.; Calleja, G. Co/Ni mixed-metal sited MOF-74 material as hydrogen adsorbent. *Int. J. Hydrogen Energy* **2015**, *40*, 5346−5352.

(19) Wang, L. J.; Deng, H.; Furukawa, H.; Gándara, F.; Cordova, K. E.; Peri, D.; Yaghi, O. M. Synthesis and characterization of metal-organic framework-74 containing 2, 4, 6, 8, and 10 different metals. *Inorg. Chem.* **2014**, *53*, 5881−5883.

(20) Khan, N. A.; Jhung, S. H. Effect of central metal ions of analogous metal-organic frameworks on the adsorptive removal of benzothiophene from a model fuel. *J. Hazard. Mater.* **2013**, *260*, 1050−1056.

(21) Song, G.; Wang, Z.; Wang, L.; Li, G.; Huang, M.; Yin, F. Preparation of MOF (Fe) and its catalytic activity for oxygen reduction reaction in an alkaline electrolyte. *Chin. J. Catal.* **2014**, *35*, 185−195.

(22) Yang, J.-M.; Liu, Q.; Sun, W.-Y. Co(II)-doped MOF-5 nano/microcrystals :solvatochromic behaviour, sensing solvent molecules and gas sorption property. *J. Solid State Chem.* **2014**, *218*, 50−55.

(23) Corma, A.; García, H.; Llabrés i Xamena, F. X. Engineering metal organic frameworks for heterogeneous catalysis. *Chem. Rev.* **2010**, *110*, 4606−4655.

(24) Dhakshinamoorthy, A.; Garcia, H. Catalysis by metal nanoparticles embedded on metal-organic frameworks. *Chem. Soc. Rev.* **2012**, *41*, 5262−5284.

(25) El-Dafrawy, S. M.; Salama, R. S.; El-Hakam, S. A.; Samra, S. E. Bimetal-organic frameworks (Cu_x-Cr_{100-x}−MOF) as a stable and efficient catalyst for synthesis of 3, 4-dihydropyrimidin-2-one and 14-phenyl-14H-dibenzo [a, j] xanthene. *J. Mater. Res. Technol.* **2020**, *9*, 1998−2008.

(26) Kholdeeva, O. A.; Skobelev, I. Y.; Ivanchikova, I. D.; Kovalenko, K. A.; Fedin, V. P.; Sorokin, A. B. Hydrocarbon oxidation over Fe- and Cr-containing metal-organic frameworks MIL-100-a comparative study. *Catal. Today* **2014**, *238*, 54−61.

(27) Anirudhan, T. S.; Sreekumari, S. S. Adsorptive removal of heavy metal ions from industrial effluents using activated carbon derived from waste coconut buttons. *J. Environ. Sci.* **2011**, *23*, 1989−1998.

(28) Fu, F.; Wang, Q. Removal of heavy metal ions from wastewaters: a review. *J. Environ. Manage.* **2011**, *92*, 407−418.

(29) Ge, F.; Li, M.-M.; Ye, H.; Zhao, B.-X.; Zhao, B.-X. Effective removal of heavy metal ions Cd^{2+}, Zn^{2+}, Pb^{2+}, Cu^{2+} from aqueous solution by polymer-modified magnetic nanoparticles. *J. Hazard. Mater.* **2012**, *211−212*, 366−372.

(30) Narayanan, S. L.; Arunkumar, C.; Perumal, R.; Saravanan, P.; Rasad, A. A. A batch study on the removal of nickel (II) using low cost adsorbent flyash. *Int. J. Chem. Petrochem. Technol.* **2014**, *4*, 31−36.
(31) Pan, S.; Shen, H.; Xu, Q.; Luo, J.; Hu, M. Surface mercapto engineered magnetic Fe_3O_4 nanoadsorbent for the removal of mercury from aqueous solutions. *J. Colloid Interface Sci.* **2012**, *365*, 204−212.
(32) Fernández-Nava, Y.; Ulmanu, M.; Anger, I.; Marañón, E.; Castrillón, L. Use of granular bentonite in the removal of mercury (II), cadmium (II) and lead (II) from aqueous solutions. *Water, Air, Soil Pollut.* **2011**, *215*, 239−249.
(33) Dong, L.; Zhu, Z.; Qiu, Y.; Zhao, J. Removal of lead from aqueous solution by hydroxyapatite/magnetite composite adsorbent. *Chem. Eng. J.* **2010**, *165*, 827−834.
(34) Nageswar, Y. V. D.; Reddy, K. H. V.; Ramesh, K.; Murthy, S. N. Recent developments in the synthesis of quinoxaline derivatives by green synthetic approaches. *Org. Prep. Proced. Int.* **2013**, *45*, 1−27.
(35) Bendale, A. R.; Patel, N.; Narkhede, S. P.; Narkhede, S. B.; Jadhav, A. G.; Vidyasagar, G. Sonochemical Synthesis of 2, 3-diphenylquinoxaline using different catalysts, a green chemistry approach. *Asian J. Res. Chem.* **2011**, *4*, 887−889.
(36) Abu-Hashem, A. A. Synthesis, reactions and biological activity of quinoxaline derivatives. *Am. J. Org. Chem.* **2015**, *5*, 14−56.
(37) Wang, L.; Liu, J.; Tian, H.; Qian, C. Ytterbium triflate catalyzed heterocyclization of 1,2-phenylenediamines and alkyl oxalates under solvent-free conditions via phillips reaction: a facile synthesis of quinoxaline-2,3-diones derivatives. *Synth. Commun.* **2004**, *34*, 1349−1357.
(38) Bandyopadhyay, D.; Mukherjee, S.; Rodriguez, R. R.; Banik, B. K. An effective microwave-induced iodine-catalyzed method for the synthesis of quinoxalines via condensation of 1, 2-diamines with 1, 2-dicarbonyl compounds. *Molecules* **2010**, *15*, 4207−4212.
(39) Hojati, S. F.; Nematdoust, Z.; Zeinali, T. The preparation of quinoxaline and 2,3-dihydropyrazine derivatives using selectfluor as an efficient and reusable catalyst. *Iran. Chem. Commun.* **2015**, *3*, 6−15.
(40) Mohammadi Ziarani, G.; Badiei, A.-R.; Azizi, M. The one-pot synthesis of 14-aryl-14H-dibenzo[a,j] xanthene derivatives using sulfonic acid functionalized silica (SiO_2-Pr-SO_3H) under solvent free conditions. *Sci. Iran.* **2011**, *18*, 453−457.
(41) Sajjadifar, S.; Fadaeian, M.; Bakhtiyari, M.; Rezayati, S. One-pot synthesis of xanthene derivatives using silica supported [2 (sulfooxy) ethyl] sulfamic acid as a novel and efficient catalyst under solvent-free condition. *Chem. Sci. Trans.* **2014**, *3*, 107−116.
(42) Paliwal, P.; Jetti, S. R.; Bhatewara, A.; Kadre, T.; Jain, S. Catalyzed synthesis of xanthene derivatives in aqueous media. *ISRN Org. Chem.* **2013**, *2013*, 526173.
(43) Heravi, M. M.; Alinejhad, H.; Bakhtiari, K.; Saeedi, M.; Oskooie, H. A.; Bamoharram, F. F. Solvent −free synthesis of xanthene derivatives by preyssler type heteropolyacid. *Bull. Chem. Soc. Ethiop.* **2011**, *25*, 399−406.
(44) Karami, B.; Hoseini, S. J.; Eskandari, K.; Ghasemi, A.; Nasrabadi, H. Synthesis of xanthene derivatives by employing Fe_3O_4 nanoparticles as an effective and magnetically recoverable catalyst in water. *Catal. Sci. Technol.* **2012**, *2*, 331−338.
(45) Cele, M. N.; Friedrich, H. B.; Bala, M. D. Liquid phase oxidation of n-octane to C_8 oxygenates over modified Fe-MOF-5 catalysts. *Catal. Commun.* **2014**, *57*, 99.
(46) Song, P.; Li, Y.; Li, W.; He, B.; Yang, J.; Li, X. A highly efficient Co (0) catalyst derived from metal-organic framework for the hydrolysis of ammonia borane. *Int. J. Hydrogen Energy* **2011**, *36*, 10468−10473.
(47) Bagherzadeh, M.; Ashouri, F.; Đaković, M. Synthesis, characterizations and catalytic studies of anew two-imensional metal-organic framework based on Co-carboxylate secondary building units. *J. Solid State Chem.* **2015**, *223*, 32−37.
(48) Hamidipour, L.; Farzaneh, F. Cobalt metal organic framework as an efficient heterogeneous catalyst for the oxidation of alkanes and alkenes. *React. Kinet. Mech. Catal.* **2013**, *109*, 67−75.
(49) Sargazi, G.; Afzali, D.; Ghafainazari, A.; Saravani, H. Rapid synthesis of cobalt metal organic framework. *J. Inorg. Organomet. Polym. Mater.* **2014**, *24*, 786−790.
(50) Wang, H.; Yin, F.; Li, G.; Chen, B.; Wang, Z. Preparation, characterization and bifunctional catalytic properties of MOF (Fe/Co) catalyst for oxygen reduction/evolution reactions in alkaline electrolyte. *Int. J. Hydrogen Energy* **2014**, *39*, 16179−16186.
(51) Brozek, C. K.; Dincă, M. Ti^{3+}, $V^{2+/3+}$, $Cr^{2+/3+}$, Mn^{2+}, and Fe^{2+} substituted MOF-5 and edox reactivity in Cr- and Fe-MOF-5. *J. Am. Chem. Soc.* **2013**, *135*, 12886−12891.
(52) Nayak, S.; Harms, K.; Dehnen, S. New three-dimensional metal-organic framework with heterometallic [Fe-Ag] building units: synthesis, crystal structure, and functional studies. *Inorg. Chem.* **2011**, *50*, 2714−2716.
(53) Wang, L. J.; Deng, H.; Furukawa, H.; Gándara, F.; Cordova, K. E.; Peri, D.; Yaghi, O. M. Synthesis and characterization of metal−organic framework-74 containing 2, 4, 6, 8, and 10 different metals. *Inorg. Chem.* **2014**, *53*, 5881−5883.
(54) Dang, G. H.; Vu, Y. T. H.; Dong, Q. A.; Le, D. T.; Truong, T.; Phan, N. T. S. Quinoxaline synthesis via oxidative cyclization reaction using metal-organic framework Cu(BDC) as an efficient heterogeneous catalyst. *Appl. Catal., A* **2015**, *491*, 189−195.
(55) Reddi Mohan Naidu, K.; Satheesh Krishna, B.; Anil Kumar, M.; Arulselvan, P.; Ibrahim Khalivulla, S.; Lasekan, O. Design, synthesis and sntiviral potential of 14-aryl/heteroaryl-14H-dibenzo [a,j] xanthenes using an efficient polymer-supported catalyst. *Molecules* **2012**, *17*, 7543−7555.
(56) Kundu, K.; Nayak, S. Camphor-10-sulfonic acid catalyzed condensation of 2-naphthol with aromatic/aliphatic aldehydes to 14-aryl/alkyl-14H-dibenzo [a,j] xanthenes. *J. Serb. Chem. Soc.* **2014**, *79*, 1051−1058.
(57) Dhakshinamoorthy, A.; Alvaro, M.; Garcia, H. Aerobic oxidation of styrenes catalyzed by an iron metal organic framework. *ACS Catal.* **2011**, *1*, 836−840.
(58) Meng, F.; Fang, Z.; Li, Z.; Xu, W.; Wang, M.; Liu, Y.; Zhang, J.; Wang, W.; Zhao, D.; Guo, X. Porous Co_3O_4 materials prepared by solid-state thermolysis of a novel Co-MOF crystal and their superior energy storage performances for supercapacitors. *J. Mater. Chem. A* **2013**, *1*, 7235−7241.
(59) Zhao, L.-H.; Yang, A.-H.; Quan, Y.-P.; Gao, H.-L.; Cui, J.-Z. 3D metal−organic framework based on cadmium complex of pyrazine-2, 3, 5, 6-tetracarboxylic acid. *J. Chem. Crystallogr.* **2011**, *41*, 1245−1248.
(60) Zhang, Z.-H.; Xu, L.; Jiao, H. Ionothermal synthesis, structures, properties of cobalt-1, 4-benzenedicarboxylate metal−organic framework. *J. Solid State Chem.* **2016**, *238*, 217−222.
(61) Liu, X.; Jingyan, W.; Li, Q.; Jiang, S.; Tianhao, Z.; Shengfu, J. Synthesis of rare earth Metal-Organic frameworks (Ln-MOFs) and their properties of adsorption desulfurization. *J. Rare Earths* **2014**, *32*, 189−194.
(62) Li, S.-X.; Feng-Ying, Z.; Yang, H.; Jian-Cong, N. Thorough removal of inorganic and organic mercury from aqueous solutions by adsorption on Lemna minor powder. *J. Hazard. Mater.* **2011**, *186*, 423−429.
(63) Azzam, A. M.; El-Wakeel, S. T.; Mostafa, B. B.; El-Shahat, M. F. Removal of Pb, Cd, Cu and Ni from aqueous solution using nano scale zero valent iron particles. *J. Environ. Chem. Eng.* **2016**, *4*, 2196−2206.
(64) Ramana, D. K. V.; Reddy, D. H. K.; Kumar, B. N.; Harinath, Y.; Seshaiah, K. Removal of Nickel from Aqueous Solutions by citric acid modified Ceiba pentandra hulls: equilibrium and kinetic studies. *Can. J. Chem. Eng.* **2012**, *90*, 111−119.
(65) Anbia, M.; Kargosha, K.; Khoshbooei, S. Heavy metal ions removal from aqueous media by modified magnetic mesoporous silica MCM-48. *Chem. Eng. Res. Des.* **2015**, *93*, 779−788.
(66) Salehin, S.; Aburizaiza, A. S.; Barakat, M. Activated carbon from residual oil fly ash for heavy metals removal from aqueous solution. *Desalination Water Treat.* **2016**, *57*, 278−287.

https://doi.org/10.1021/acsomega.2c01770
ACS Omega 2022, 7, 23421−23444

(67) Parida, K.; Mishra, K. G.; Dash, S. K. Adsorption of toxic metal ion Cr (VI) from aqueous state by TiO2-MCM-41: Equilibrium and kinetic studies. *J. Hazard. Mater.* **2012**, *241*−*242*, 395−403.
(68) Masindi, V.; Gitari, W. M. Simultaneous removal of metal species from acidic aqueous solutions using cryptocrystalline magnesite/bentonite clay composite: an experimental and modelling approach. *J. Clean. Prod.* **2016**, *112*, 1077−1085.
(69) Jain, M.; Garg, V. K.; Kadirvelu, K.; Sillanpää, M. Adsorption of heavy metals from multi-metal aqueous solution by sunflower plant biomass-based carbons. *Int. J. Sci. Environ. Technol.* **2016**, *13*, 493−500.
(70) Barakat, M. A.; Kumar, R. Synthesis and characterization of porous magnetic silica composite for the removal of heavy metals from aqueous solution. *Ind. Eng. Chem.* **2015**, *23*, 93−99.
(71) Ihsanullah; Abbas, A.; Al-Amer, A. M.; Laoui, T.; Al-Marri, M. J.; Nasser, M. S.; Khraisheh, M.; Atieh, M. A. Heavy metal removal from aqueous solution by advanced carbon nanotubes: critical review of adsorption applications. *Sep. Purif. Technol.* **2016**, *157*, 141−161.
(72) Mahapatra, A.; Mishra, B. G.; Hota, G. Electrospun Fe_2O_3-Al_2O_3 nanocomposite fibers as efficient adsorbent for removal of heavy metal ions from aqueous solution. *J. Hazard. Mater.* **2013**, *258*−*259*, 116−123.
(73) Bediako, J. K.; Wei, W.; Kim, S.; Yun, Y.-S. Removal of heavy metals from aqueous phases using chemically modified waste Lyocell fiber. *J. Hazard. Mater.* **2015**, *299*, 550−561.
(74) Bandyopadhyay, D.; Mukherjee, S.; Rodriguez, R. R.; Banik, B. K. An effective microwave-induced iodine-catalyzed method for the synthesis of quinoxalines via condensation of 1,2-diamines with 1,2-dicarbonyl compounds. *Molecules* **2010**, *15*, 4207−4212.
(75) Dang, G. H.; Vu, Y. T. H.; Dong, Q. A.; Le, D. T.; Truong, T.; Phan, N. T. S. Quinoxaline synthesis via oxidative cyclization reaction using metal−organic framework Cu(BDC) as an efficient heterogeneous catalyst. *Appl. Catal., A* **2015**, *491*, 189−195.
(76) Kumar, S.; Khan, S. A.; Alam, O.; Azim, R.; Khurana, A.; Shaquiquzzaman, M.; Siddiqui, N.; Ahsan, W. Synthesis of tetrazolo [1, 5-a] quinoxaline based azetidinones & thiazolidinones as potent antibacterial & antifungal agents. *Bull. Korean Chem. Soc.* **2011**, *32*, 2260−2266.
(77) Lü, H.-Y.; Deng, S. H.; Zhang, Z. H. Magnetic Fe_3O_4 nanoparticles as new efficient, and reusable catalysts for the synthesis of quinoxaline in water. *Aust. J. Chem.* **2010**, *63*, 1290−1296.
(78) Chang, B.; Fu, J.; Tian, Y.; Dong, X. Mesoporous solid acid catalysts of sulfated zirconia/SBA-15 derived from a vapor−induced hydrolysis route. *Appl. Catal., A* **2012**, *437*−*438*, 149−154.
(79) El-Hakam, S. A.; Samra, S. E.; El-Dafrawy, S. M.; Ibrahim, A. A.; Salama, R. S. Surface acidity and catalytic activity of sulfated titania supported on mesoporous MCM-41. *Int. J. Mod. Chem. Appl. Sci.* **2013**, *5*, 55−70.
(80) Kour, M.; Paul, S.; Clark, J. H.; Gupta, V. K.; Kant, R. Preparation and characterization of lewis acid grafted sulfonated carbon@ titania composites for the multicomponent synthesis of 4 H pyrimido[2,1-b] Benzothiazoles and Benzoxanthenones under solvent-free conditions. *J. Mol. Catal. A: Chem.* **2016**, *411*, 299−310.
(81) EL-Dafrawy, S. M.; Hassan, S. M.; Farag, M. Kinetics and mechanism of Pechmann condensation reaction over sulphated zirconia-supported zinc oxide. *J. Mater. Res. Technol.* **2020**, *9*, 13−21.
(82) Mahadik, P.; Jagwani, D.; Joshi, R. A greener chemistry approach for synthesis of 2, 3-diphenyl quinoxaline. *J. Innovat. Sci. Eng. Technol.* **2014**, *1*, 482−490.
(83) Rajabi, F.; Alves, D.; Luque, R. An Efficient and Recyclable Nanoparticle-Supported Cobalt Catalyst for Quinoxaline Synthesis. *Molecules* **2015**, *20*, 20709−20718.
(84) Karami, B.; Hoseini, S. J.; Eskandari, K.; Ghasemi, A.; Nasrabadi, H. Synthesis of xanthene derivatives by employing Fe_3O_4 nanoparticles as an effective and magnetically recoverable catalyst in water. *Catal. Sci. Technol.* **2012**, *2*, 331−338.

https://doi.org/10.1021/acsomega.2c01770
ACS Omega 2022, 7, 23421−23444